DAHLGREN DIVISION
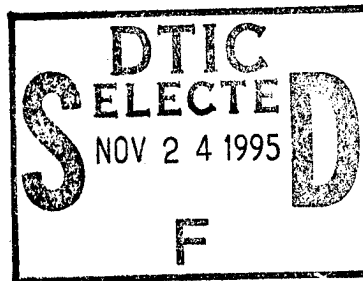# NAVAL SURFACE WARFARE CENTER
Dahlgren, Virginia 22448-5100

NSWCDD/TR-94/351

PRELIMINARY ANALYSIS OF VERTICAL-MOTION DETECTION FOR LOW-ELEVATION TARGETS WITH DOPPLER PROCESSING AT W-BAND

BY G. W. GROVES   J. E. CONTE   W. D. BLAIR

SYSTEMS RESEARCH AND TECHNOLOGY DEPARTMENT

DTIC
SELECTED
NOV 2 4 1995
F

OCTOBER 1995

19951121 056

DTIC QUALITY INSPECTED 5

FOREWORD

Tracking low-elevation, highly maneuverable targets at short range with fire control accuracy is a high-priority problem for ship self-defense. This technical note examines the possibility of detecting target vertical motion by using W-band Doppler information on low-elevation targets in the presence of multipath propagation. Low-elevation targets are difficult to track because large errors occur in the elevation measurements during the multipath nulls, which are characterized by a lower signal-to-noise ratio. A level-flying target appears to perform large maneuvers in the vertical plane during the multipath nulls. The presence of these nulls makes it difficult to ascertain if a target is performing an actual maneuver.

In the presence of multipath reflections, the returning scattered signals are shifted in frequency by amounts that are different for the directly reflected and the sea-surface reflected rays. If the difference between the shifted frequencies can be detected in the presence of spectral broadening resulting from a variable range rate and limited resolution, the difference can be used to obtain more accurate target position determinations. Only certain types of trajectories have radial velocity components such that the target and its multipath image can be both detected and distinguished. If W-band Doppler processing can be used to detect vertical motion of low-elevation targets, it will provide an important contribution to ship self-defense.

The present study was supported by the Surface Weapons Systems Technology Program, managed at NSWCDD by Robin Staton. This technical report was reviewed by Dr. Theodore R. Rice, B-32.

Accesion For	
NTIS CRA&I	☑
DTIC TAB	☐
Unannounced	☐
Justification	
By	
Distribution /	
Availability Codes	

Dist	Avail and / or Special
A-1	

Approved by:

Mary E. Lacey, Acting Head
Systems Research and Technology Department

ABSTRACT

The detection of vertical motion of a low-elevation target in multipath by frequency analysis using millimeter waves such as W-band radar is considered. Target vertical motion can be detected if the range rate of the image differs sufficiently from that of the target itself, so that their Doppler shifts allow resolution of the target return from its image. This observed difference in frequency provides additional information on target position and velocity. The favorable circumstances that create the possibility of using this effect to detect vertical target motion are discussed. An optimum interval in the time domain for analysis is developed for the case when the multipath-induced splitting of the Doppler-shifted frequencies is resolvable. A procedure is outlined for determining at each radar dwell (1) whether or not the multipath returns are resolvable, and (2) the appropriate analysis interval for achieving the resolution. A practical signal-processing technique is suggested for achieving the desired spectral resolution. Several examples of target trajectories are presented to illustrate cases where each method succeeds or fails. Conclusions and recommendations for further studies are given.

CONTENTS

ILLUSTRATIONS

CHAPTER 1

INTRODUCTION

The range rate of a constant-speed target and consequently also the Doppler shift depend on the flight-path angle relative to the radar. Thus, changes in the flight-path angle can be detected by Doppler measurements. Measurements of Doppler frequency shift have been used along with measurements of target range, elevation, and azimuth in the Kalman filtering process to provide more accurate state estimates than would be achieved by using position measurements alone. Maneuvers that are associated with a change in target acceleration are more readily detected through measurements of velocity than by measurements of position. Here, we wish to consider other ways in which measurements of Doppler can provide additional clues regarding target motion. One way involves making use of the difference in range rate of a low-elevation target and its multipath image. This effect is enhanced by using millimeter-wave radar (*i.e.*, W band).

Besides using this Doppler shift in the Kalman process to enhance the accuracy of the state estimates, it can be used within the Interactive Multiple Model algorithm to provide better model or mode detection. For example, while tracking a target in approximately level flight, a sudden decrease in Doppler shift might indicate a diving or ascending maneuver and trigger an emphasis on the *maneuver* mode. The same concept is valid in a three-dimensional trajectory, where the shift in Doppler could be related to azimuthal motion as well as change in flight-path angle. To accommodate more complicated scenarios, the appropriate algorithms would be developed to use the Doppler measurements in this additional way.

To use the small difference in Doppler shifts between the target and its multipath image, several conditions need to be satisfied to obtain useful results. A simple way of relating these frequency shifts is to consider two functions, the target slant range $\rho(t)$ and the path-length difference (PLD), $s(t)$, which is equal to the image slant range minus the target slant range. There are three paths by which a radar signal emitted from the transmitter can echo from the target and return to the receiving antenna. These are (1) the *Direct-Direct* (DD) path of length 2ρ with no sea reflection, (2) the *Direct-Reflected* (DR) or the *Reflected-Direct* (RD) path of length $2\rho + s$ with one sea reflection, and (3) the *Reflected-Reflected* (RR) path of length $2(\rho + s)$ with two sea reflections. Accordingly, under ideal conditions there would be three distinct Doppler shifts in frequency (the difference between the DR and the RD

shift being always too small to be detected). Since s is usually only a few centimeters for a low-E target, it is necessary that the rate of variation of s be appreciable. To a rough approximation, $|ds/dt|$ is larger for a sharply ascending or diving target. It is also possible for the target to fly along the surfaces of equal PLD to make it impossible to resolve the image Doppler from the target Doppler. Another difficulty is *Acceleration Broadening* of the Doppler lines caused by variation in range rate during the interval over which the harmonic analysis is performed. In many situations, this effect makes it impossible to resolve the three Doppler shifts.

In cases where the multipath frequency shifts can be resolved from the skin shift, the results of the frequency analysis can be used in two ways. First, the amount of splitting provides an estimate of ds/dt, which could be considered as an additional measurement and factored into the Kalman update to provide a more accurate estimated state. Secondly, the target peak contains no contribution from rays reflected from the sea surface, and thus is not affected by multipath. Even in situations where the multipath shifts are not completely resolvable, a small number of Fourier coefficients near the combined Doppler frequency may contain sufficiently different information in the sum and difference channels to allow some *purification* of the total return from the part contributed by sea reflections. To implement this concept, those Fourier coefficients would possibly be treated as additional observations in the filtering scheme.

To make use of these effects, considerations of radar technology, the kinematics of the target trajectory, and issues of signal processing all need to be examined. A preliminary discussion of these matters is given in subsequent chapters. The important matter of atmospheric effects including ducting are not considered at this time. Note that the figures appear at the end of each chapter.

CHAPTER 2

DOPPLER SHIFT OF MULTIPATH IMAGE

In multipath there are four ray paths over which the transmitted signal can reach the target and return to the receiving antenna. Let these be designated DD, DR, RD, and RR, for Direct-Direct, Direct-Reflected, etc. If ρ is the target slant range, then these four paths have total lengths given by

DD	2ρ
DR	$2\rho + s$
RD	$2\rho + s$
RR	$2\rho + 2s$

where s has been called the PLD and is defined as

$$s = \rho_a + \rho_t - \rho \qquad (2.1)$$

where ρ_a is the distance from the antenna to the specular sea reflection point, and ρ_t is distance from the specular sea reflection point to the target. For a low-flying target and shipboard antenna, the PLD is only a few centimeters. Figure 2-1 displays the PLD as a function of target range and target height, which may be denoted by the function $s(\rho, H)$, where the implicit dependence on Earth radius and antenna height is not indicated. The frequency shift caused by Doppler is proportional to the time rate of change of these four ray paths. The motion of a target affects these rates of change through the velocity components $d\rho/dt$ and dH/dt, where H is target height and t is time.

Reflection from the sea surface is complicated and poorly understood. A simplified model studied by Northam[1] considers the reflected signal as consisting of two components. The first is the *specular* component, which is a wave that would be reflected from a flat mirror with a certain reflection coefficient. The second is the *diffuse* component, which is composed of the reflections from many facets of the irregular water surface, which is more conveniently treated statistically. The specular component suffers a phase reversal upon reflection, and thus the phase received at the antenna is determined by the total round-trip path length plus the phase reversal. The phase of the diffuse component is treated as a stochastic variable with uniform distribution on $[0, 2\pi)$. The discussion presented here considers only the specular component.

The effect of target motion on the Doppler-shifted radar signal has been studied by Gray[2]. If the motion is consistent with a constant range rate, then the Doppler effect produces a shift in frequency. (Otherwise, the more complete treatment of Chapter 4 is necessary.) It is convenient to consider the difference of the frequency shifts of the reflected rays relative to that of the DD ray, which is just the ordinary skin Doppler shift given by

$$f_d = -\frac{2f}{c}\frac{d\rho}{dt} \tag{2.2}$$

These relative multipath shifts are

$$\text{for DR or RD} \rightarrow \Delta f_1 = -\frac{f}{c}\left[\frac{\partial s}{\partial \rho}\frac{d\rho}{dt} + \frac{\partial s}{\partial H}\frac{dH}{dt}\right]$$

$$\text{for RR} \rightarrow \Delta f_2 = -\frac{2f}{c}\left[\frac{\partial s}{\partial \rho}\frac{d\rho}{dt} + \frac{\partial s}{\partial H}\frac{dH}{dt}\right] \tag{2.3}$$

where c is the speed of light and f is the frequency of the transmitted radar signal. The gradient components that enter the relations (Equation (2.3)) can be readily computed. The relations for sea reflection on a spherical Earth are[3,4]

$$\rho_t(2ah + h^2 - \rho_a^2) = \rho_a(2aH + H^2 - \rho_t^2) \tag{2.4}$$

and

$$a^2[(\rho_a + \rho_t)^2 - \rho^2] = (2ah + h^2 - \rho_a^2)(2aH + H^2 - \rho_t^2) \tag{2.5}$$

where a is the radius of the Earth and h is antenna height, as denoted in Equation (2.2). These equations, which can be used to determine ρ_a and ρ_t when the other quantities are known, were used to construct Figure 2-1. The components of the gradient of s can be determined by differentiating Equations (2.4) and (2.5) with respect to ρ while keeping H constant. Thus,

$$[-2\rho_a\rho_t - 2aH - H^2 + \rho_t^2]\frac{\partial \rho_a}{\partial \rho} + [2ah + h^2 - \rho_a^2 + 2\rho_a\rho_t]\frac{\partial \rho_t}{\partial \rho} = 0$$

$$[a^2(\rho_a + \rho_t) + (2aH + H^2 - \rho_t^2)\rho_a]\frac{\partial \rho_a}{\partial \rho}$$

$$+[a^2(\rho_a + \rho_t) + (2ah + h^2 - \rho_a^2)\rho_t]\frac{\partial \rho_t}{\partial \rho} = a^2\rho \tag{2.6}$$

which is a linear equation in the gradient components. If Equations (2.4) and (2.5) are differentiated with respect to H keeping ρ constant, the same coefficient matrix is obtained for the gradient components $\partial \rho_a/\partial H$ and $\partial \rho_t/\partial H$, where the equations are now

$$[-2\rho_a\rho_t - 2aH - H^2 + \rho_t^2]\frac{\partial \rho_a}{\partial H} + [2ah + h^2 - \rho_a^2 + 2\rho_a\rho_t]\frac{\partial \rho_t}{\partial H} = 2(a + H)\rho_a$$

$$[a^2(\rho_a + \rho_t) + (2aH + H^2 - \rho_t^2)\rho_a]\frac{\partial \rho_a}{\partial H}$$

$$+[a^2(\rho_a + \rho_t) + (2ah + h^2 - \rho_a^2)\rho_t]\frac{\partial \rho_t}{\partial H} = (a + H)(2ah + h^2 - \rho_a^2)$$

$$\tag{2.7}$$

The components of the gradient of s are then obtained from Equation (2.1). The results are shown in Figures 2-3 and 2-4. Figure 2-3 shows a family of curves representing the range component of the PLD gradient as a function of target range, for target heights of 2.5, 5.0, 7.5,..., 25 m. Figure 2-4 shows the family of curves for the height component of the gradient of the PLD for the same height values.

Consider an example where an incoming threat is located at a range of 6 km and a height of 10 m with a range rate of -300 m/s and rising at a rate of 10 m/s. The target is observed with a 100 GHz radar signal. From Figures 2-3 and 2-4 the PLD gradient components are $\partial s/\partial \rho = -1.1 \times 10^{-5}$ and $\partial s/\partial H = 6 \times 10^{-3}$. With the given threat velocity, Equation (2.3) gives $\Delta f \simeq (3.3 \times 10^{-3} + 6 \times 10^{-2})f/c \simeq 20$ Hz. The Doppler shifts for the target itself and the two multipath shifts are thus 200 kHz, 200.02 kHz, and 200.04 kHz. In this example, the threat is rising and is therefore crossing the iso-PLD surfaces at a faster rate than if it were in level flight. The vertical component of the threat velocity contributes more to this shift than the horizontal component. If the threat wished to minimize the Doppler shift, it would fly down along one of the iso-PLD surfaces during the final phase of flight where the PLD gradient becomes large.
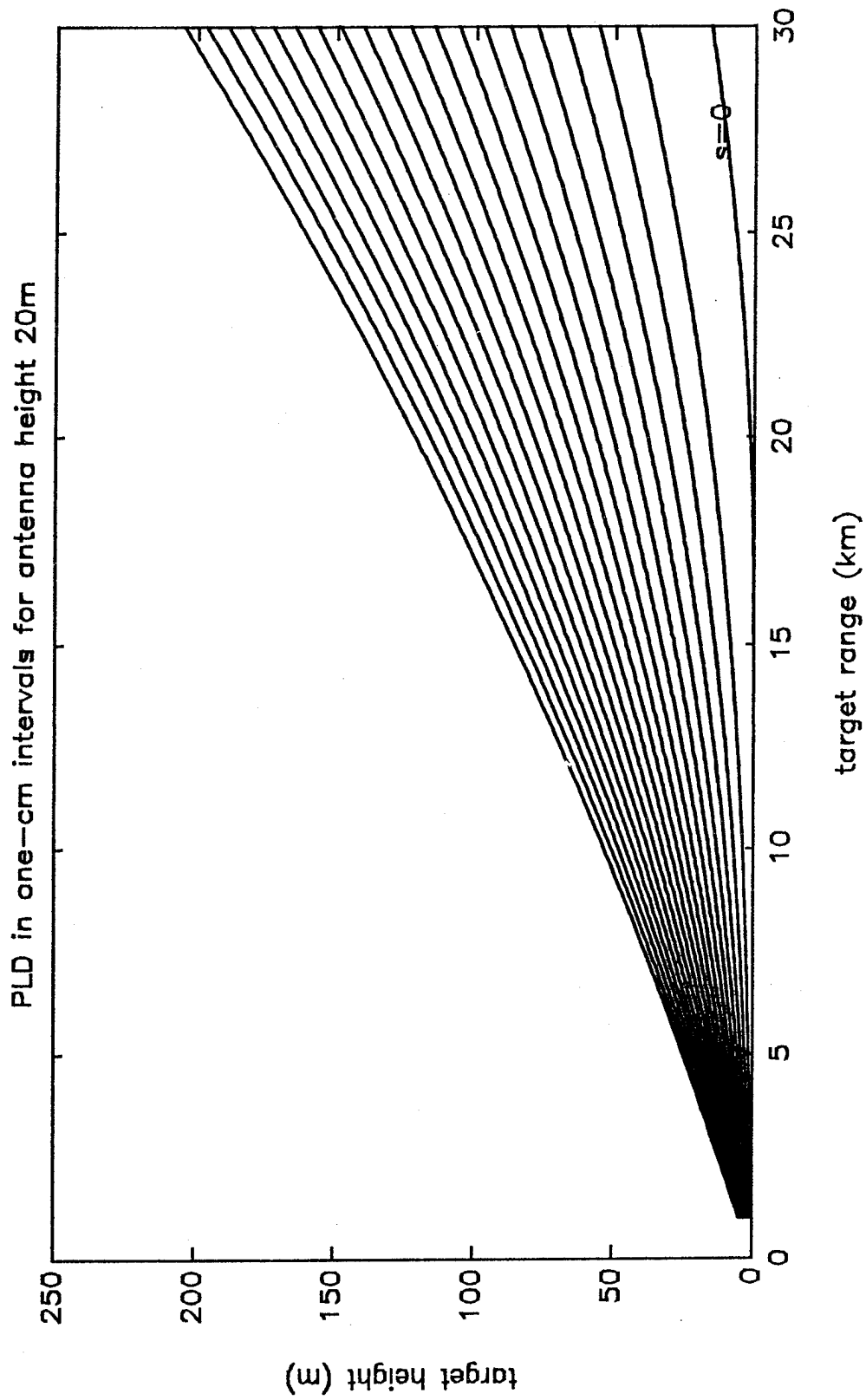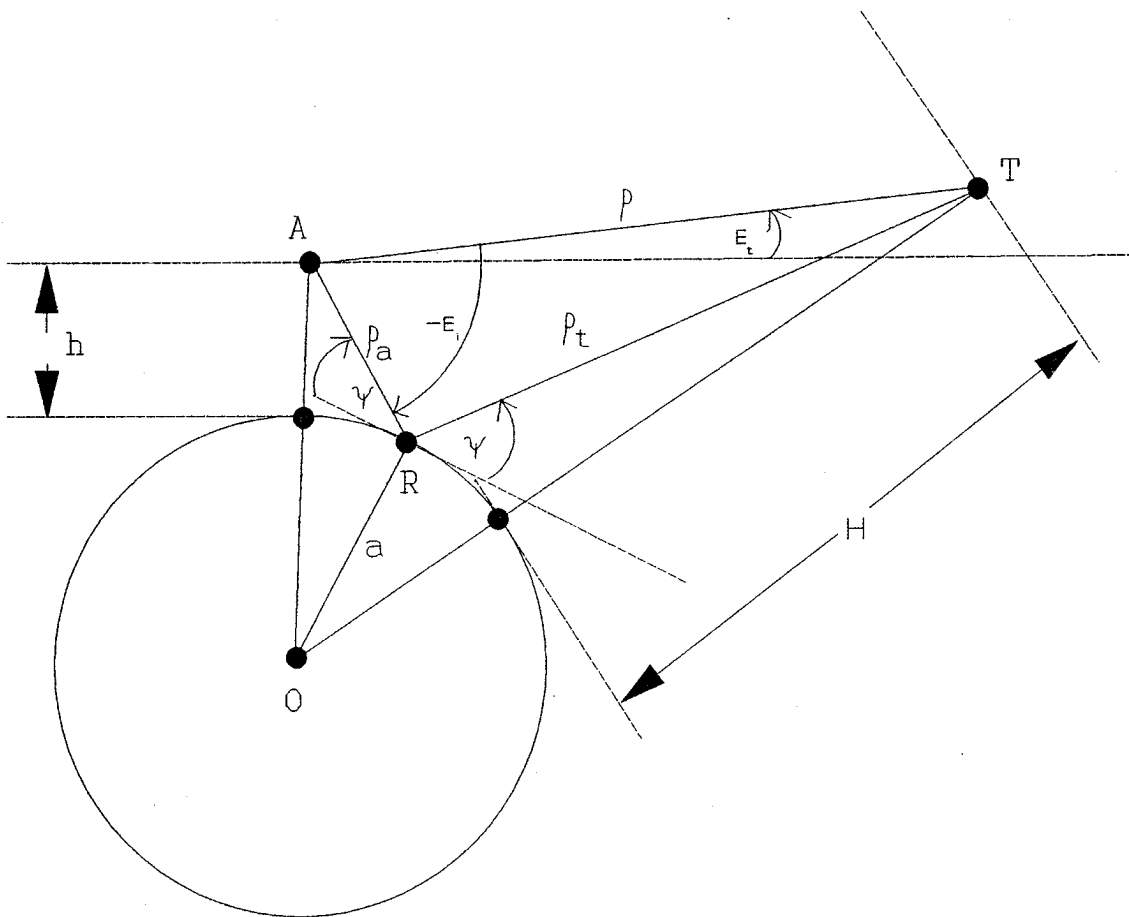
Figure 2-1. Field of Path-Length Difference

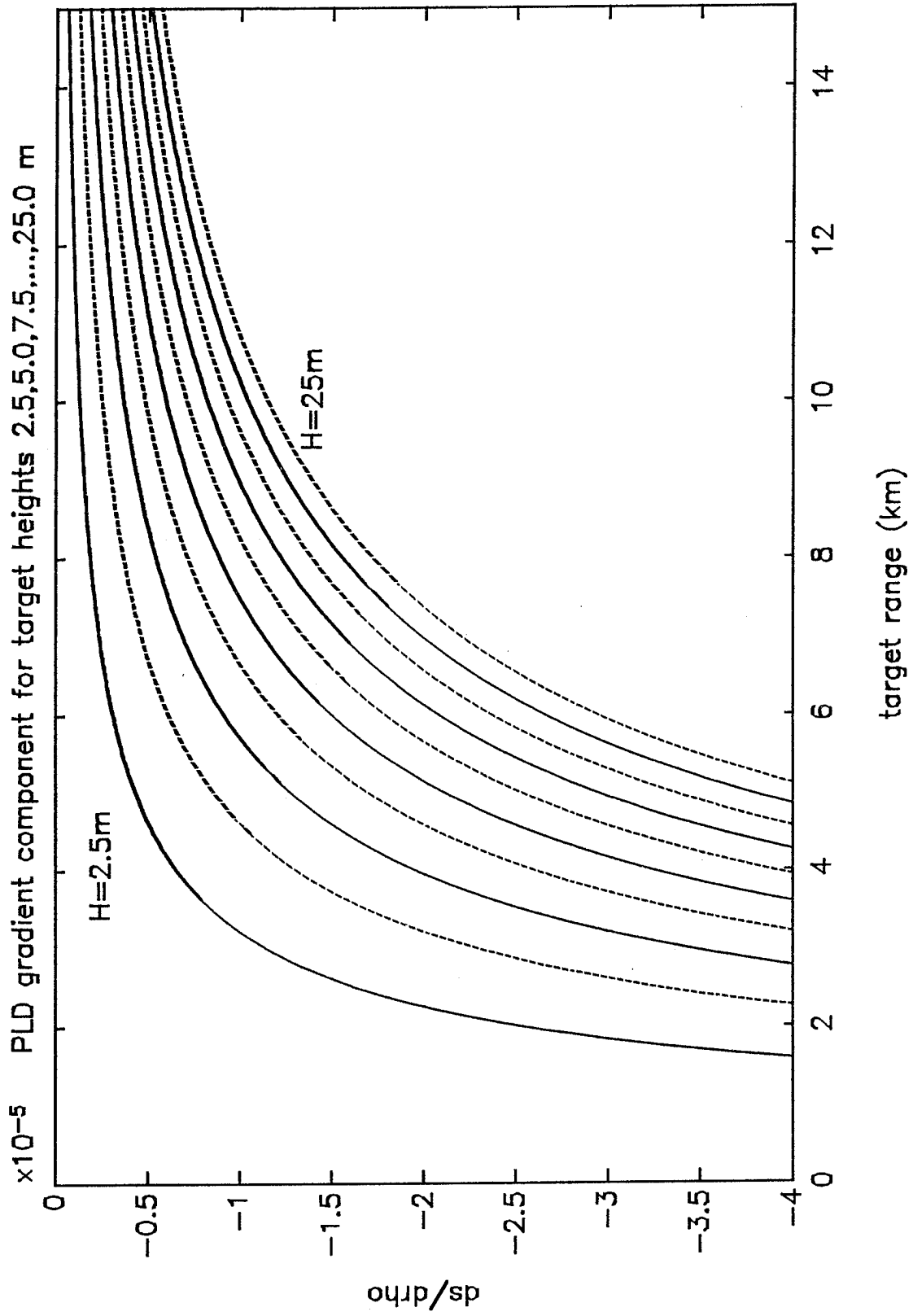Figure 2-2.   Geometry of sea reflection
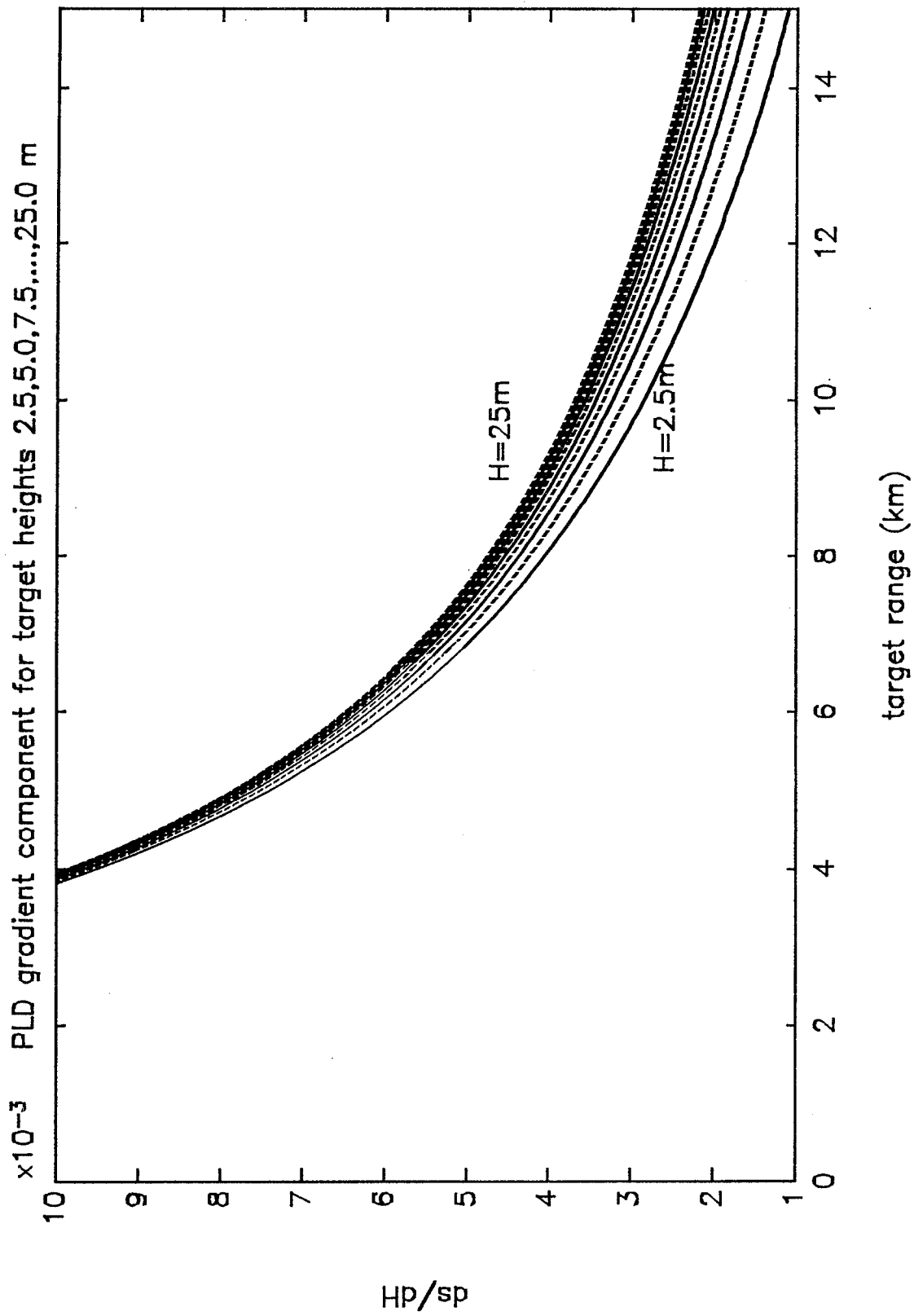
Figure 2-3. Range Component of PLD Gradient

Figure 2-4.   Height Component of PLD Gradient

CHAPTER 3

SIGNAL PROCESSING METHODS AND ISSUES

The Doppler signal will have to be processed in such a way as to achieve a resolution of about 8 Hz to render observable the separation of the frequency lines due to multipath effects during acceleration. The following is a suggested method for this processing.

The frequencies of interest are expected to be within 60 to 120 Hz of the line associated with the true target Doppler (*i.e.*, the skin line). The analog signal should be mixed down to a center frequency that is BW/2 less than the skin line, where BW is a selected bandwidth centered on the skin line. A rough estimate of the skin line value can be obtained from the tracking filter range rate. By allowing BW to be much larger than 120 Hz (say 15.565 kHz), there is little chance that the frequency lines of interest will be shifted too much (*i.e.*, into the negative frequency band) and become aliased. Once the mixing is accomplished, the signal can be sampled at 2 BW. If BW is 15.565 kHz, an N-point FFT will then give a frequency resolution of $\Delta f = 7.6$ Hz, if N=2(15565)/7.6 = 4096 points. With this high resolution periodogram, the skin line frequency can then be found again, with much higher accuracy than was done using the track filters. The separate frequency line due to the multipath can then be searched for within a ± 120-Hz band about the skin line frequency. This process is illustrated in Figure 3-1.

Since the multipath Doppler lines are so close to the skin line, some concerns associated with this method include the effects of windowing and airframe vibration. First, sidelobes associated with the skin line will be present, due to the rectangular window resulting from the finite length of the data sequence. The sidelobes may be of sufficient amplitude to obscure the multipath Doppler lines. If a time window is applied to reduce the sidelobes, the mainlobe will grow wider. This widening may also obscure the multipath lines. Perhaps an optimal time window will have to be chosen to minimize the effects of this problem.

Another issue is airframe vibration. Since the airframe may vibrate with a natural frequency on the order of 20 to 100 Hz, there is a question as to whether the vibrational frequencies will obscure the separation of the spectral lines due to multipath. The lowest mode, near 20 Hz should be dominant. Since it is a sinusoidal motion, lines due to vibration should appear on both sides of the skin frequency. Lines due to multipath should appear only on one side of the skin frequency. This information could permit the vibrational lines

to be ignored or removed during processing. Cepstral processing could possibly be applied to locate and remove the vibrational lines in a manner similar to echo removal from audio signals, but some distortion of the desired signal will result[5]. It remains to be determined whether or not the amount of this distortion can be tolerated.

This analysis has thus far neglected the effects of *acceleration broadening* of the skin line. This is not directly related to physical acceleration and can occur even when the target is not accelerating, as in Case Study 3 in Chapter 5. It is caused by a nonuniform range rate resulting in a nonvanishing $\ddot{\rho}$, where the dots indicate time derivatives. Since the quantity $\ddot{\rho}$ is readily estimated from repeated measurements of range and/or Doppler, and has the dimensions of acceleration, it is given the name *range pseudoacceleration* and is expressed in g units when convenient. It is related to true physical acceleration in an indirect way. It is recalled that in polar coordinates (ρ, E) the radial component of acceleration is given by $\ddot{\rho} - \rho \dot{E}^2$, where the second term is the centripetal acceleration. Thus, it can be written (range pseudoacceleration) = (radial acceleration) + (centripetal acceleration). A discussion of acceleration broadening in the case of nonuniform target motion is given in Reference 6. A constant range pseudoacceleration of just one g may cause a single Doppler spectrum line to broaden to a width of 200 Hz at W band. Obviously, the three spectral lines cannot be resolved with this much overlap when the separation is only about 20 Hz. To avoid acceleration broadening, the target must follow a trajectory having small range pseudoacceleration. It is clear that the multipath Doppler lines can be resolved only in certain special circumstances.

These circumstances are roughly that the multipath splitting must be larger than the acceleration broadening and larger than the spectral separation, which is the difference in frequency required for two spectral lines to be resolvable by the signal-processing used. The multipath splitting is the frequency interval between any two adjacent multipath Doppler-shifted frequencies, as given by Equation (2.3) or deducible from Equations (4.6) and (4.8). The acceleration broadening is as described in the previous paragraph. This suggests the existence of two *Resolution Parameters* defined by

$$P_1 = \left| \frac{\text{multipath splitting}}{\text{acceleration broadening}} \right|, \qquad P_2 = \left| \frac{\text{multipath splitting}}{\text{spectral separation}} \right| \qquad (3.1)$$

The multipath splitting, acceleration broadening, and spectral separation are expressed in terms of the width of a frequency range and are given by $f_0 \dot{s}/c$, $2f_0(\dot{\rho}_{max} - \dot{\rho}_{min})/c$, and $1/T_a$, respectively, where $\dot{\rho}_{max}$ and $\dot{\rho}_{min}$ are the maximum and minimum range rates occurring during the analysis time interval T_a. If a constant range pseudoacceleration is assumed during the analysis interval, then $\dot{\rho}_{max} - \dot{\rho}_{min}$ can be replaced by $\ddot{\rho} T_a$. With these definitions, the Resolution Parameters are given by

$$P_1 = \left| \frac{\dot{s}}{\ddot{\rho} T_a} \right|, \qquad P_2 = \left| \frac{f_0 \dot{s} T_a}{c} \right| \qquad (3.2)$$

Of course, the multipath lines themselves can undergo broadening related to a nonvanishing $\ddot{s}$, which would also exacerbate the problem of resolution. To be more precise, the definition of P_1 in (3.2) should replace $|\ddot{\rho}|$ by $|\ddot{\rho}| + |\ddot{s}|$. But since s and its time derivatives are not measured directly, and since the definitions (Equation (3.5)) are inexact and useful only as a guide, this change is not recommended.

In order to err on the conservative side when $\dot{s}$ or $\ddot{\rho}$ is not constant during the analysis interval, the minimum value of $|\dot{s}|$ and the maximum value of $|\ddot{\rho}|$ should be used. Then

$$P_1 = \frac{|\dot{s}|_{\min}}{|\ddot{\rho}|_{\max}T_a}, \qquad P_2 = \frac{f_0|\dot{s}|_{\min}T_a}{c} \tag{3.3}$$

According to these definitions, it is necessary that $P_1 > 1$ and $P_2 > 1$, (probably $P_1 \gg 1$ and $P_2 \gg 1$), in order that the multipath Doppler signals be resolvable.

It is noted that a longer analysis interval improves the spectral separation but worsens the acceleration broadening. Thus, an optimum T_a can be found by equating P_1 and P_2, with the result being

$$T_{\text{opt}} = \sqrt{\frac{c}{f_0|\ddot{\rho}|_{\max}}} \tag{3.4}$$

When this optimum analysis interval is used, the Resolution Parameters attain their optimum (*i.e. best compromise*) value

$$P_{\text{opt}} = |\dot{s}|_{\min}\sqrt{\frac{f_0}{c|\ddot{\rho}|_{\max}}} \tag{3.5}$$

The general procedure is to examine the value of P_{opt} in Equation (3.5). If this value does not comfortably exceed unity, then no analysis interval will resolve the multipath lines. If the value of P_{opt} does exceed unity, then there is an optimum T_a given by Equation (3.4). If $T_a < T_d$, where T_d is the dwell interval, then the data can be divided into segments of interval T_a and analyzed. A waterfall representation of the results will show the multipath lines resolved. Alternatively, a more sophisticated time-frequency analysis[7,8] will also achieve the desired resolution. If $T_a > T_d$, insufficient data are available to achieve an optimum resolution, but if the value of P_2 in Equation (3.3) comfortably exceeds unity, an analysis over the T_d interval will still resolve the multipath lines.
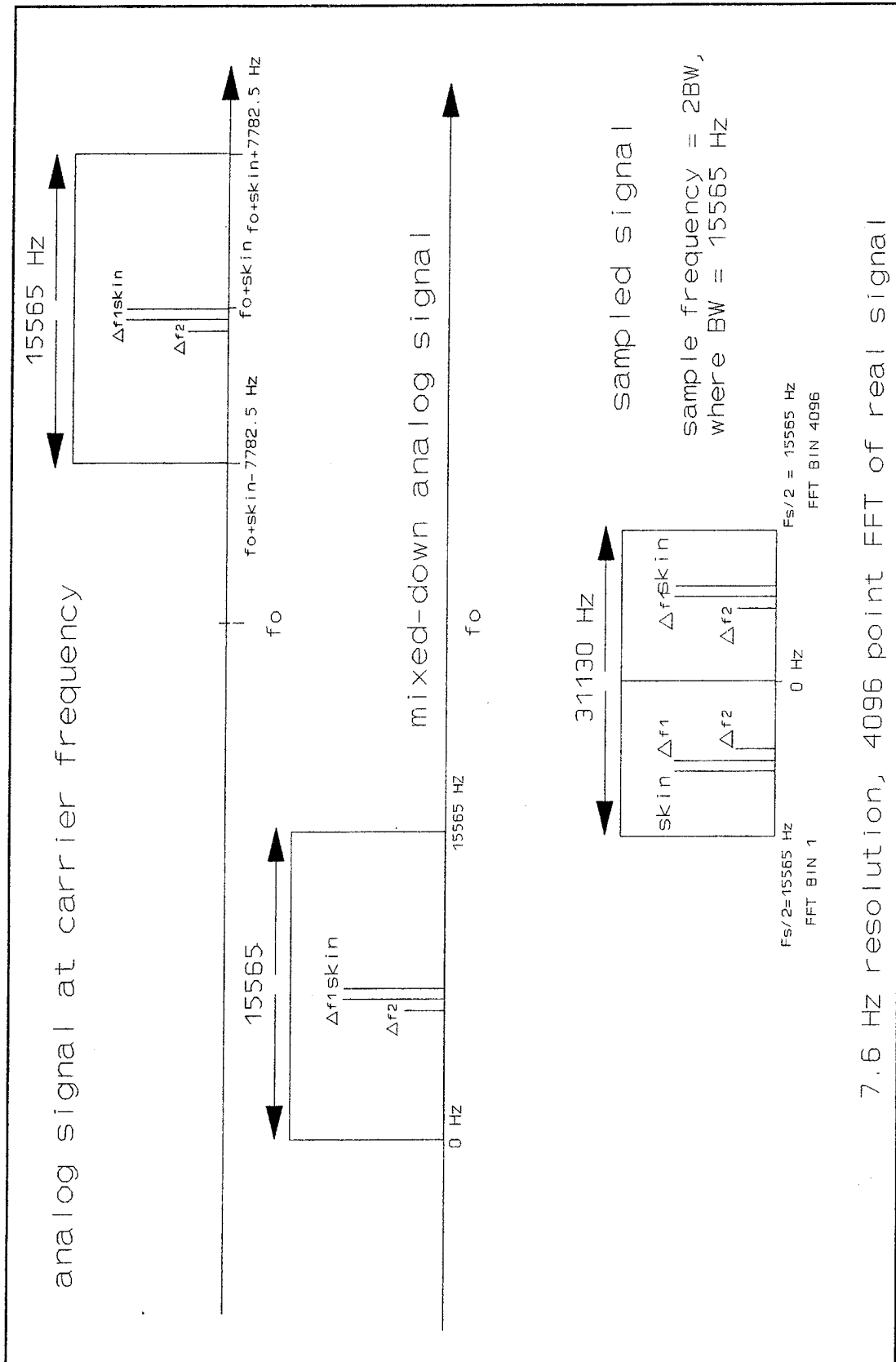
Figure 3-1. The mixing and Samping Process to Achieve Desired Resolution

CHAPTER 4

SCATTERED SIGNAL RECEIVED FROM A MOVING POINT TARGET IN MULTIPATH

CONTINUOUS WAVE DOPPLER

It is assumed that the radar is emitting a continuous unmodulated wave, allowing the echo signals to be received at any desired time. The situation with pulsed Doppler is deferred until later. The target trajectory is assumed specified, and it is required to determine the nature of the scattered signals returning to the antenna. The only trajectory information needed to determine the variation of phase (*i.e.*, frequency) of the returning signal is the time history of the target slant range $\rho(t)$ and path-length difference $s(t)$. When the time rate of change of the slant range and PLD are constant, the simplified discussion of Chapter 2 is valid, but here the functions $\rho(t)$ and $s(t)$ are general. The variation of amplitude of the returning signal is not being considered. A signal returning to the receiving antenna at time t will have been emitted and scattered off the target at the times given in Table 4-1 for the four ray paths, where $\rho_{DD}(t)$ is the target slant range at the time when the signal returning at time t along the DD ray was being scattered at the target, and similarly for $\rho_{DR}(t)$, $\rho_{RD}(t)$, and $\rho_{RR}(t)$.

Table 4-1. RAY CHRONOLOGY

Ray Path	Scattered at Time	Emitted at Time
DD	$t - \rho_{DD}/c$	$t - 2\rho_{DD}/c$
DR	$t - (\rho_{DR} + s)/c$	$t - (2\rho_{DR} + s)/c$
RD	$t - \rho_{RD}/c$	$t - (2\rho_{RD} + s)/c$
RR	$t - (\rho_{RR} + s)/c$	$t - 2(\rho_{RR} + s)/c$

Let the emitted signal of amplitude A be represented by

$$V(t) = A \cos(\omega t) \tag{4.1}$$

Then according to Table 4-1, the signal that reaches the target at time t along the DD ray is

$$U_{DD}(t) = AKV(t - 2\rho_{DD}/c) = AK \cos[\omega(t - 2\rho_{DD}/c)] \tag{4.2}$$

where K accounts for all reduction of signal strength from spreading to attenuation in air,

and is different for the different signals even though the same symbol is used. It is required to determine ρ_{DD} in terms of the given function $\rho(t)$. From Table 4-1 it is seen that

$$\rho_{DD}(t) = \rho(\tau), \quad \text{where} \quad \tau = t - \frac{\rho_{DD}(t)}{c} \tag{4.3}$$

This equation determines $\rho_{DD}(t)$, whose value can be found by successive approximations using the given function $\rho(t)$. In practical cases, the time argument on the right side of Equation (4.3) might be assumed to be displaced by a small amount from the time t, because the target displacement during the round trip of the microwaves may seem small. However, a mach-two target flying toward the radar antenna and observed by W-band radar at a distance of ten kilometers will have moved a distance of $2\rho v/c \simeq 4$ cm, where v is the range rate. This is equal to several wavelengths of a W-band signal ($\lambda \simeq 3$ mm), which is by no means negligible. Thus, it seems prudent to consider a Taylor expansion of Equation (4.3),

$$\rho_{DD}(t) = \rho(t) - \frac{\rho_{DD}(t)}{c}\dot{\rho}(t) + \frac{1}{2}\left(\frac{\rho_{DD}(t)}{c}\right)^2 \ddot{\rho}(t) + \ldots \tag{4.4}$$

The quadratic term of Equation (4.4) is of the order of tens of nanometers for a range pseudoacceleration of 10 g for the same example. This is indeed small compared to a wavelength and can be ignored. Thus, $\rho_{DD}(t)$ can be evaluated from the first two terms of Equation (4.4), and gives the result

$$\rho_{DD}(t) = \left(1 + \frac{\dot{\rho}(t)}{c}\right)^{-1}\rho(t) \simeq \left(1 - \frac{\dot{\rho}(t)}{c}\right)\rho(t) \tag{4.5}$$

neglecting higher powers of $\dot{\rho}(t)/c$. From now on, whenever the time argument is not expressed explicitly, it is understood to be t. With the approximation (Equation (4.5)) the signal $U_{DD}(t)$ can then be written as

$$U_{DD}(t) = AK \cos\left[\omega\left(t - \frac{2\rho}{c}\left(1 - \frac{\dot{\rho}}{c}\right)\right)\right] \tag{4.6}$$

When the same considerations are applied to the other rays, the results are

$$\rho_{RD} = \rho_{DD} = \left(1 - \frac{\dot{\rho}}{c}\right)\rho, \qquad \rho_{DR} = \rho_{RR} = \left(1 - \frac{\dot{\rho}}{c}\right)\rho - \frac{s\dot{\rho}}{c} \tag{4.7}$$

which gives

$$U_{DR}(t) = AK \cos\left[\omega\left(t - \frac{s}{c} + \frac{2\dot{\rho}s}{c^2} - \frac{2\rho}{c}\left(1 - \frac{\dot{\rho}}{c}\right)\right)\right]$$

$$U_{RD}(t) = AK \cos\left[\omega\left(t - \frac{s}{c} - \frac{2\rho}{c}\left(1 - \frac{\dot{\rho}}{c}\right)\right)\right] \tag{4.8}$$

$$U_{RR}(t) = AK \cos\left[\omega\left(t - \frac{2s}{c} + \frac{2\dot{\rho}s}{c^2} - \frac{2\rho}{c}\left(1 - \frac{\dot{\rho}}{c}\right)\right)\right]$$

After the foregoing approximations are made, it is noted that the functions $U_{RD}(t)$ and $U_{DR}(t)$ differ by $2\dot{\rho}s/c^2$ in the time argument. In terms of phase, this is equal to $4\pi\dot{\rho}sf/c^2$ for a radar frequency f. For W-band radar and a mach-1 approaching target with s about 20 cm, this phase difference is about 0.6 mrad and is completely negligible. Therefore, the function $U_{RD}(t)$ can be taken equal to $U_{DR}(t)$. On the other hand, the functions $U_{DD}(t)$ and $U_{DR}(t)$ differ by s/c in the time argument. The corresponding phase difference is $2\pi sf/c$, which is about 100 cycles with the previously assumed values, with another 100-cycle phase difference between $U_{DR}(t)$ and $U_{RR}(t)$. In view of the large size of these phase differences along with uncertainties in phase related to an extended target size and various noise sources, the phase relations between the three Doppler-shifted returning signals can be assumed random.

CHAPTER 5

CASE STUDIES

CASES 1 AND 2

Consider the two trajectories of Figure 5-1, which represent an incoming constant speed target with vertical maneuvers. The target initially moves with speed 300 m/s in level flight at height 5 m, rising to a height of 20 m for several kilometers, and then descending back to 5 m. The turns are with lateral acceleration of 10 m/s^2 in the first trajectory, and 60 m/s^2 in the second.

The mixed-down Doppler signals, plotted as functions of range, are shown in Figures 5-2 and 5-3. Here it is assumed that the skin line is perfectly tracked so that it is always mixed down to 1280 Hz to place it at the center of a 2560-Hz bandwidth of interest. The skin shift for the 6-g trajectory is larger because the rising and descending segments of the trajectory are steeper, which because of the constant-speed constraint causes a greater rate of decrease in the range rate.

In the level segments, the PLD is slowly increasing, which makes the image appear to approach the origin slightly slower than the target itself and consequently the multipath shifts lie below the skin shift. In the ascending segment, the PLD is increasing (see Figure 2-1) faster, which increases the difference in approach rates of the image relative to the target, reduces the Doppler shift, and lowers the multipath shifts. In the descending segment, the PLD is actually decreasing, which reverses the above effects.

In Figure 5-4, the idealized discrete Fourier transforms are shown for the two example signals at the range points corresponding to maximum spectral separation for the ascending segments of the trajectories. It has been assumed that the amplitudes of the DR and RD image signals are half that of the skin return (DD), and the RR image signal amplitude is one fourth that of the skin return. With a resolution of 5 Hz, the 1-g maneuver causes a maximum spectral separation of about 15 Hz, or 3 FFT bins, and the 6-g maneuver causes a maximum spectral separation of about 35 Hz, or 7 FFT bins.

The Resolution Parameters defined in Chapter 3 are useful in describing these phenomena. At an upward-accelerating part of the trajectory showing a 6-g turn in Figure 5-1, it is found that $P_1 = 0.12$ and $P_2 = 3.41$ for an analysis over the entire data interval of 0.13 s. The value of P_{opt} is equal to 0.63. Thus, there is no possibility of resolving the multipath lines with a better selection of T_a.

To carry out this analysis, 2^{16} time samples were generated at intervals of 2 μs, (*i.e.*, a 0.5 MHz sample rate). These were then digitally *heterodyned* to a frequency of 15.565 kHz less than the skin line by multiplying each time series by $e^{-2\pi i(f_0+f_d-BW)t}$, where BW is bandwidth. The data were then down-sampled by taking every 16th point to give a sample frequency of 2 BW=31130 Hz, as shown in Figure 3-1.

A 4096-point FFT gives a resolution of 7.6 Hz. A bandwidth larger than that used in the idealized case was required to accommodate the large spectral broadening due to acceleration.

The 6-g trajectory has the spectrum shown in Figure 5-5. Notice that the broadened spectrum for the analysis interval of 0.13 s is over 500 Hz wide. The radial velocity component of this target is not large, so that the multipath lines remain close to the skin line. This example confirms the above conclusion that the analysis interval is too long to resolve the multipath lines because of the acceleration broadening. Figure 5-6 shows what happens when T_a is reduced to its optimal value. Since P_{opt} is less than one, the multipath lines cannot be resolved because of line broadening even though the effect of the acceleration is significantly reduced.

CASE STUDY 3

This study considers the trajectory of a constant-velocity incoming target at a range of approximately 5 km, rising from near the sea surface with a flight-path angle of 60 deg and speed 660 m/s. In spite of the constant velocity, this target has a range pseudoacceleration of about 10 g. The spectra for the target and image are shown in Figure 5-7, and represents a situation in which the spectral resolution should be good because the target and images have quite different range rates. However, the massive acceleration broadening which occurs over the 0.13-s sample totally obscures this. An interesting phenomenon is seen in the *noisy plateau* of the sum spectrum. This is caused by the peculiar pattern of phase relations between the three signals.

The Resolution Parameters of this case are $P_1 = 0.45$ and $P_2 = 161$. The low value of P_1 explains the inability to resolve the multipath because of the acceleration broadening. But since P_{opt} is 8.5, an analysis over the interval $T_{\text{opt}} = 0.0069$ s can accomplish this resolution. Four such analyses over a shorter interval are shown in Figure 5-8.

An example of the effect of analysis interval on the multipath resolvability and the Resolution Parameters is illustrated in Figure 5-9. The upper plot shows an analysis over an interval of half the optimum, illustrating the broadening effect of the *sinc* response to a short analysis. The center plot is an analysis over the optimum interval, showing the resolved multipath lines. The bottom plot shows an analysis over an interval of twice the optimum to illustrate the acceleration broadening. The optimal T_a is seen to provide the best resolution of the multipath lines.

CASE STUDY 4

This study considers the trajectory of a target at a range of 10 km near the sea surface moving nearly straight up at mach 2, to keep the slant range constant. Thus, the radial pseudoacceleration and Doppler shift are zero. The spectral resolution (Figure 5-10) is good because the PLD rate and consequently the image range rate are significant. Note that the spectral multipath lines are clearly distinguishable for this 0.13- s sample.

The values of the Resolution Parameters are $P_1 = \infty$ and $P_2 = 110$ for analysis over the entire data interval, which indicates that the multipath lines are easily resolvable. The value of P_{opt} yields an analysis interval not much different than T_d.

CASE STUDY 5

This study considers a trajectory on the vertical plane having both a constant-speed and a constant-range-rate constraint. Under these conditions, the kinematic equations are

$$
\begin{aligned}
\dot{x}^2 + \dot{H}^2 &= v^2 \\
x\dot{x} + H\dot{H} &= v_r\sqrt{x^2 + H^2}
\end{aligned}
\tag{5.1}
$$

where v is the constant speed and v_r is the constant range rate (with $v_r < v$). The solution to Equation (5.1) is easily obtained in polar coordinates (r, E), where r is range and E is an elevation angle. These are related to horizontal range and height by $x = r\cos E$, $y = H\sin E$. The solution is

$$
\begin{aligned}
r(t) &= r_0 + v_r t \\
E(t) &= E_0 + \frac{\sqrt{v^2 - v_r^2}}{v_r}\ln\left(1 + \frac{v_r t}{r_0}\right)
\end{aligned}
\tag{5.2}
$$

Eliminating t gives the trajectory

$$
r = r_0 \exp\left(\frac{v_r(E - E_0)}{\sqrt{v^2 - v_r^2}}\right)
\tag{5.3}
$$

which is an exponential spiral. This trajectory has $\ddot{\rho} = 0$, which makes it easy to resolve the multipath splitting. A trajectory was formed by taking $r_0 = 10$ km, $E_0 = -0.15$ deg, $v = 330$ m/s, and $v_r = -200$ m/s. The Resolution Parameters have the values $P_1 = \infty$, $P_2 = 13$, and $P_{\text{opt}} = \infty$. An analysis was carried out over 2^{16} data at interval $dt = 2$ μs. The spectra of the mixed-down signal are shown in Figure 5-11. As expected, the skin Doppler shift is a true line, and the multipath shifts are clearly resolved. The widening observed on the multipath *lines* are the result of variation in $\dot{s}$ over the analysis interval.

example trajectory with speed 300 m/s and 1g turns

target range (km)

target height (m)

example trajectory with speed 300 m/s and 6g turns
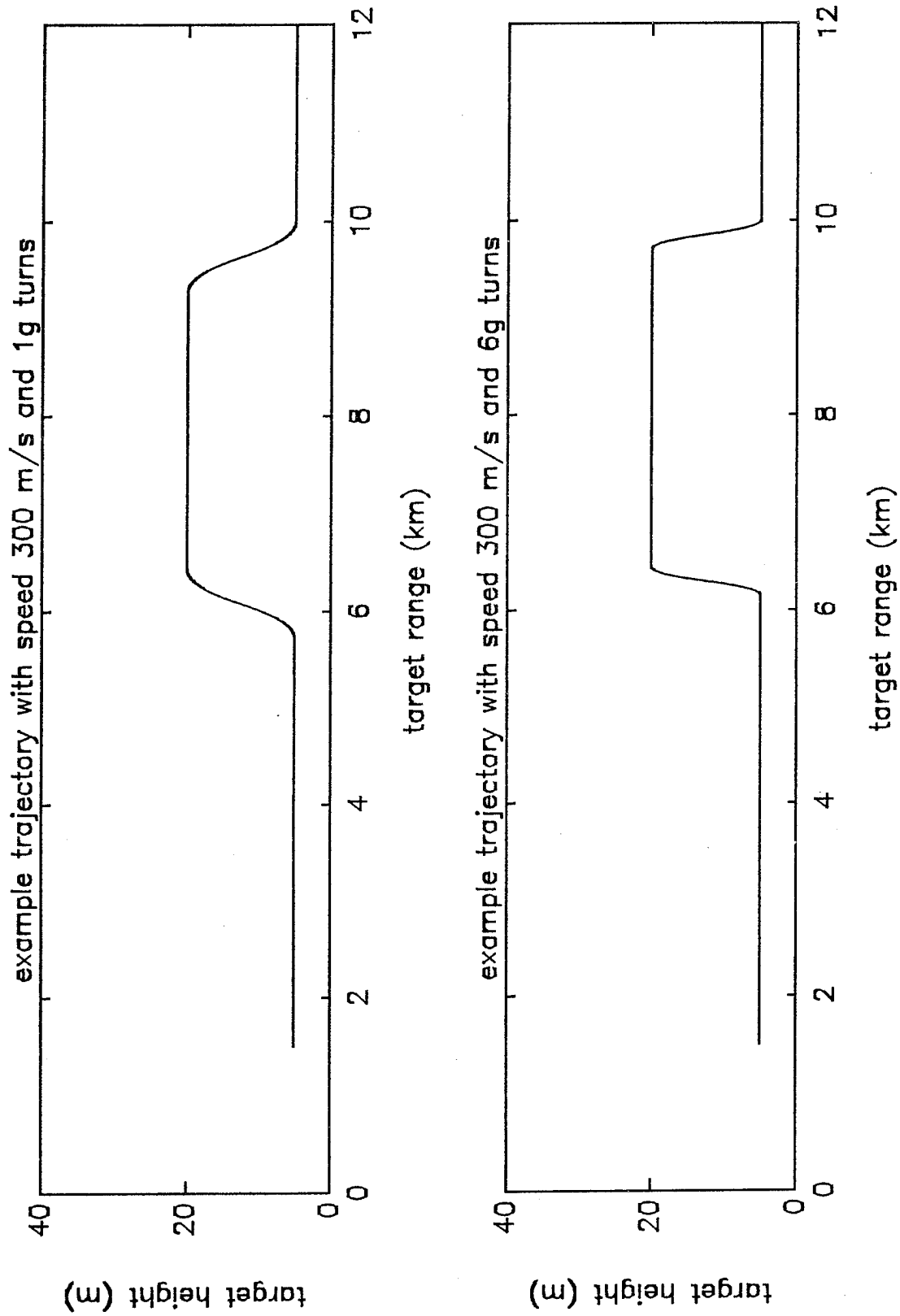
target range (km)

target height (m)
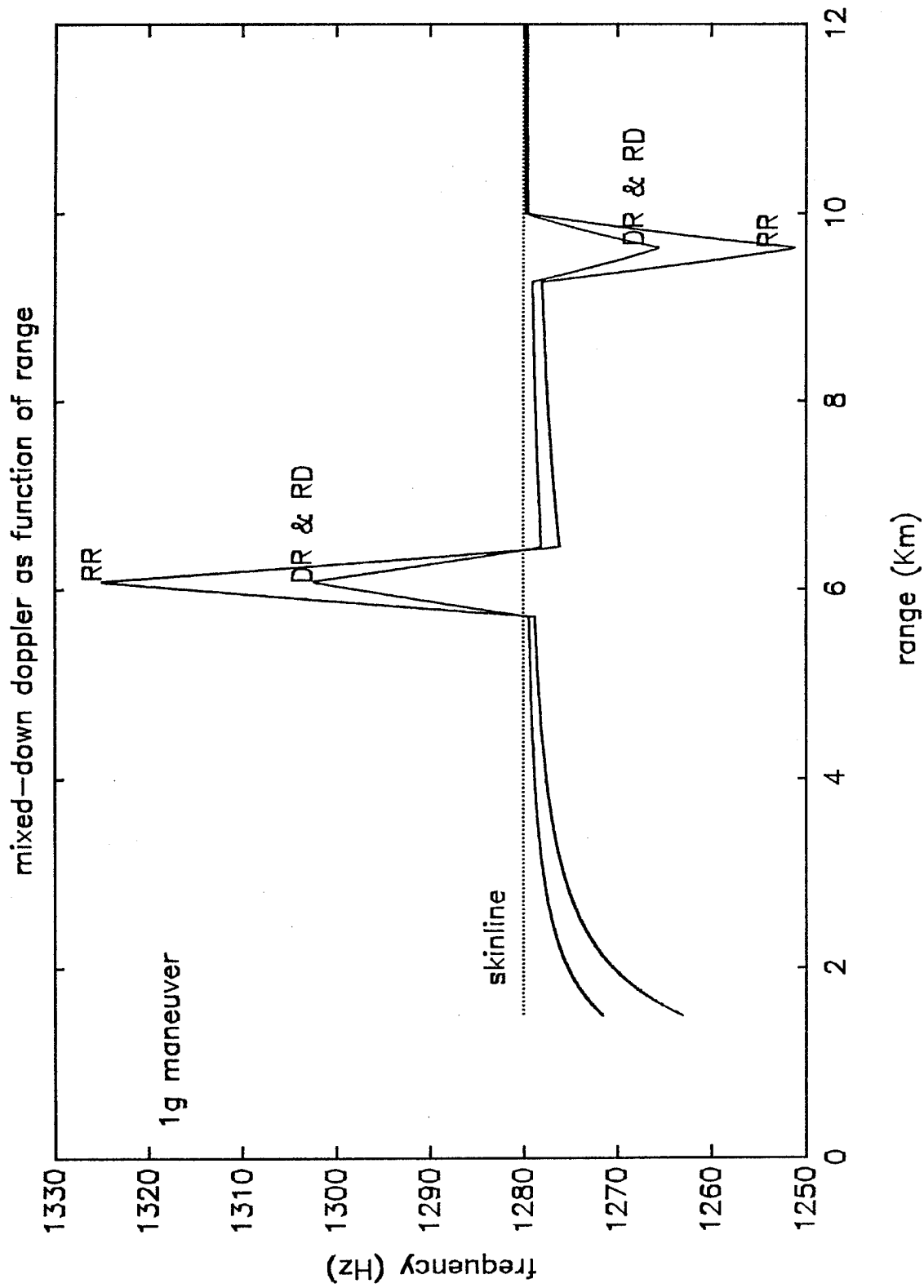
Figure 5-1. Example Trajectories

Figure 5-2.   Mixed-Down Doppler Spectrum vs Range for 1-g Maneuver
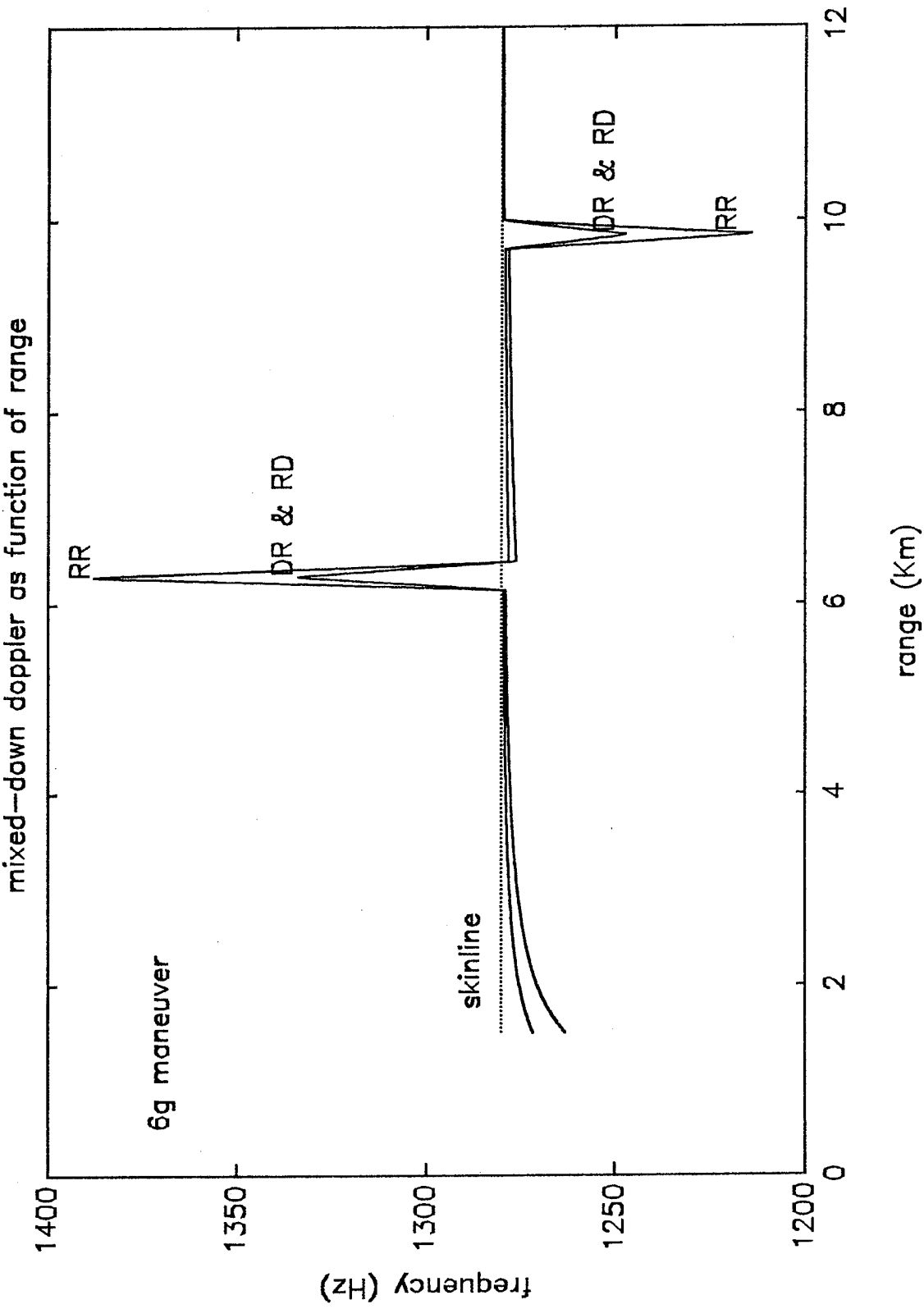
Figure 5-3. Mixed-Down Doppler Spectrum vs Range for 6-g Maneuver
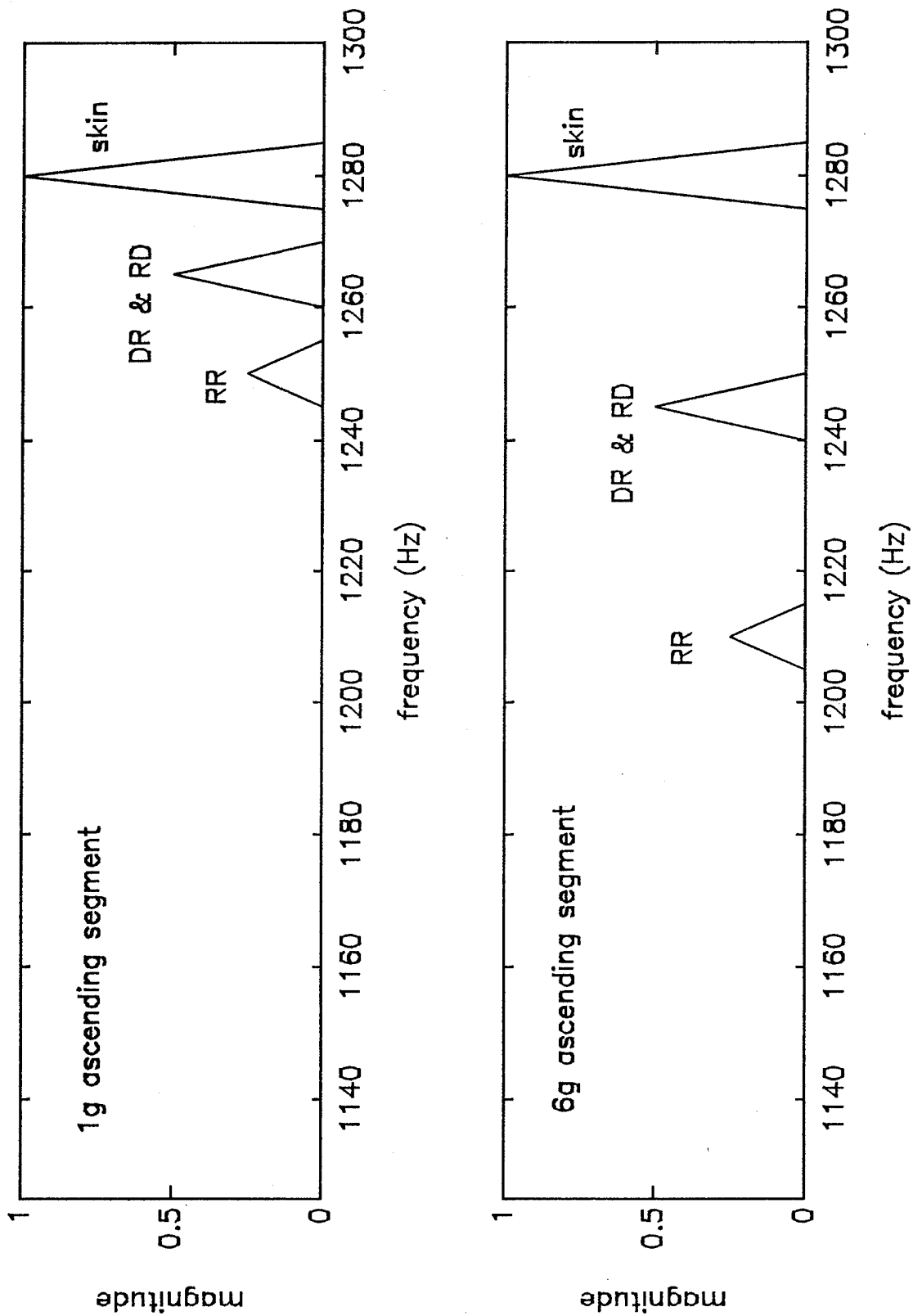
Figure 5-4. Comparison of 1-g and 6-g Idealized Doppler Spectra
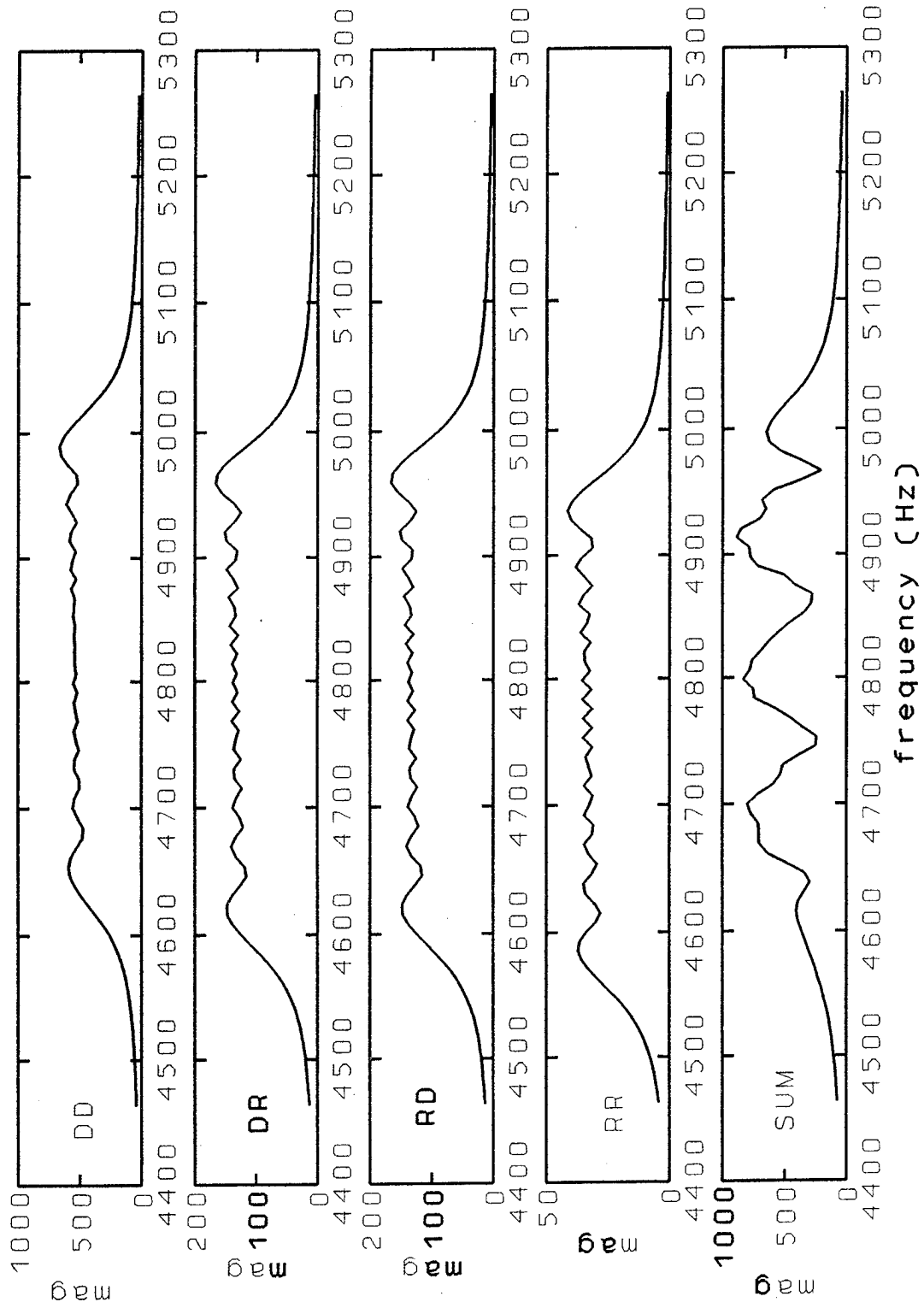
Figure 5-5. Target and Image Spectra of 6-g Target
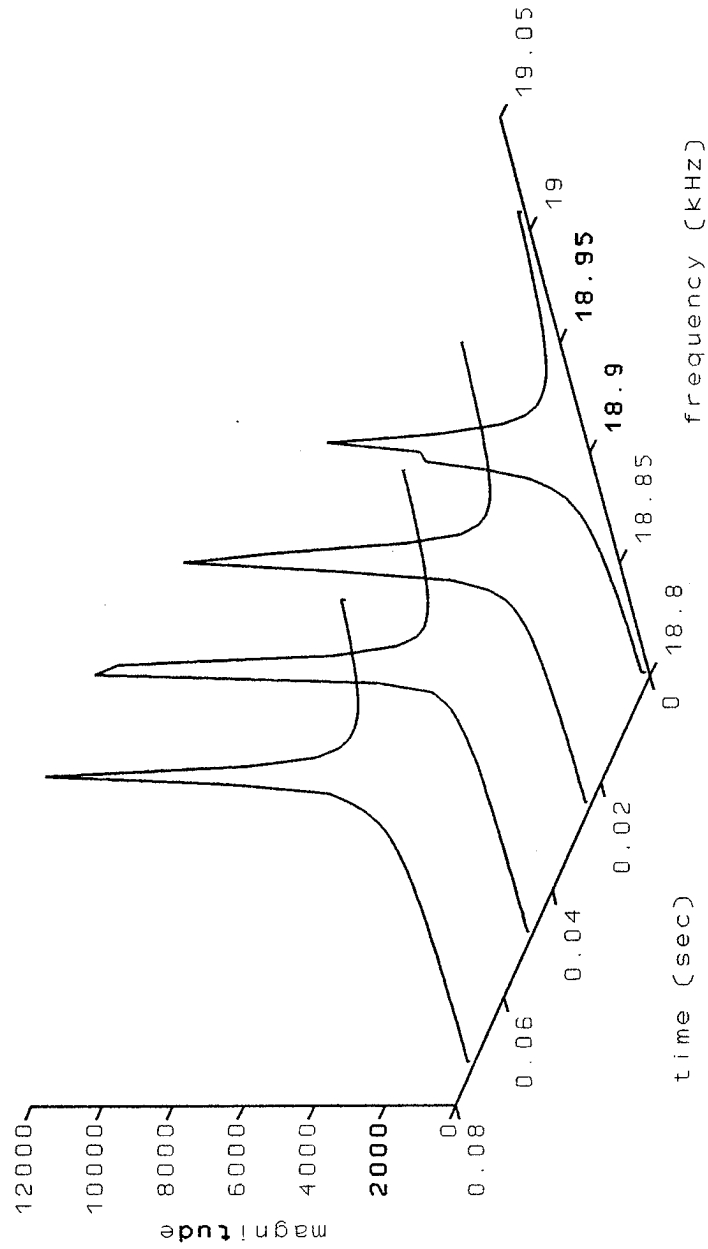
Figure 5-6. Spectra of 6-g Maneuver Using Optimum Analysis Interval
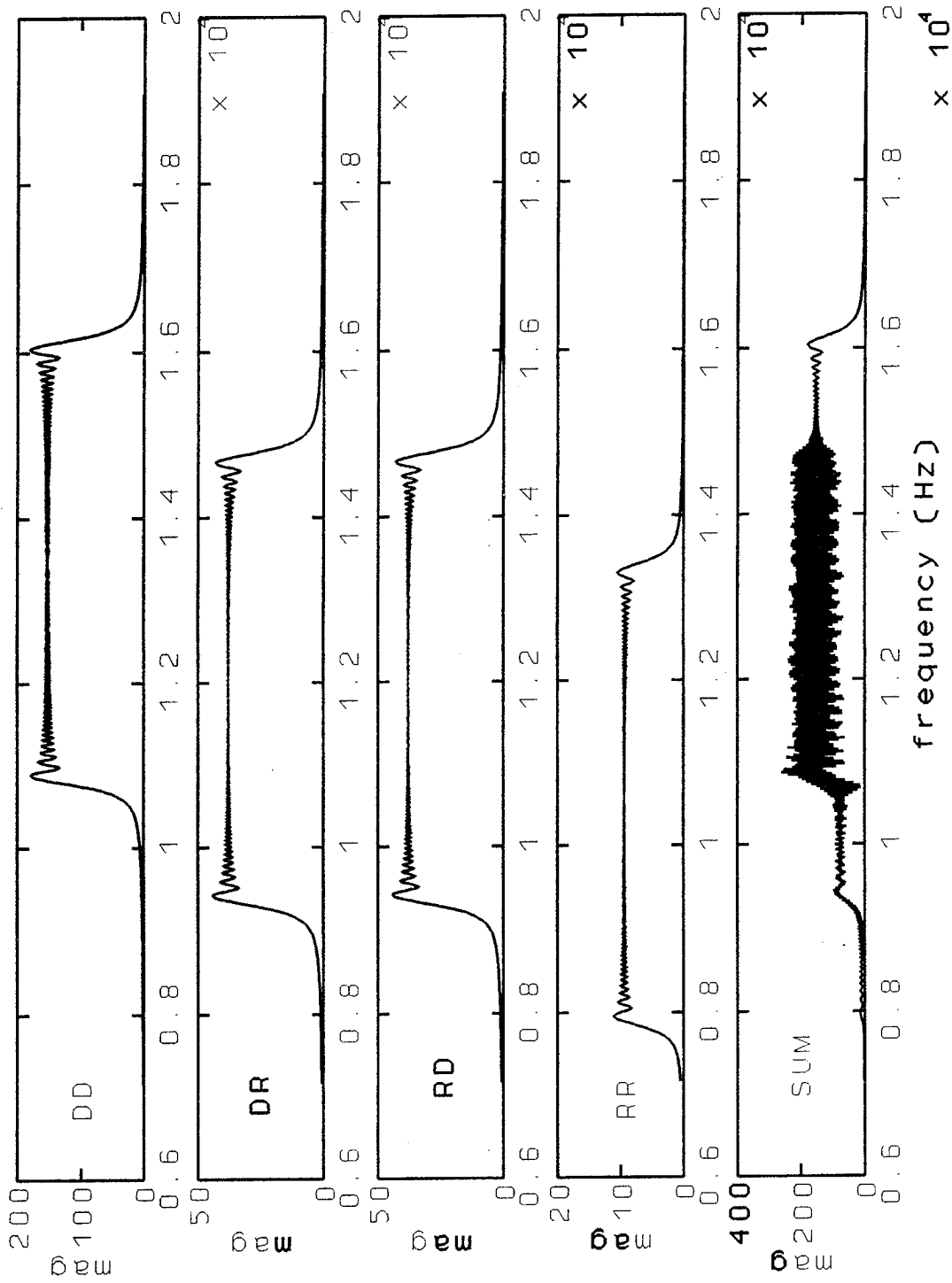
Figure 5-7. Spectra of Range-Rate 10-g Target
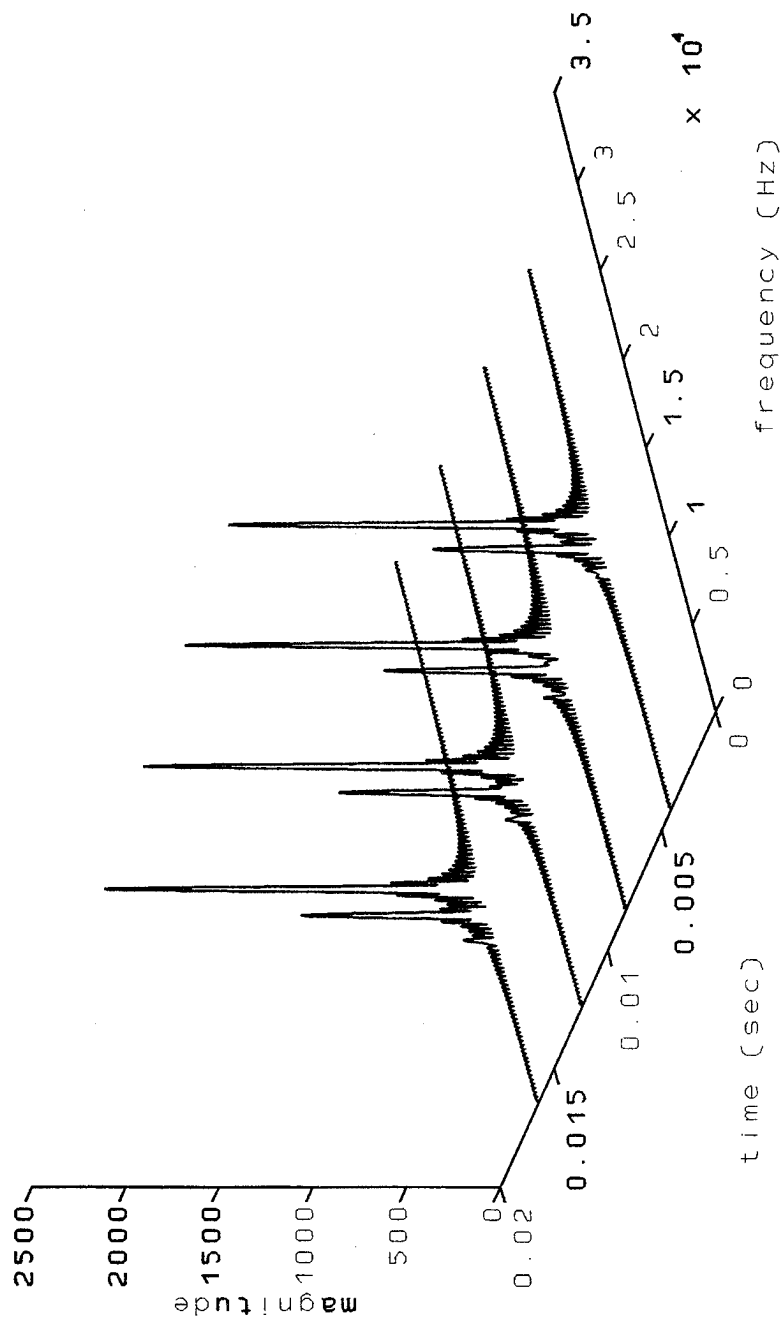
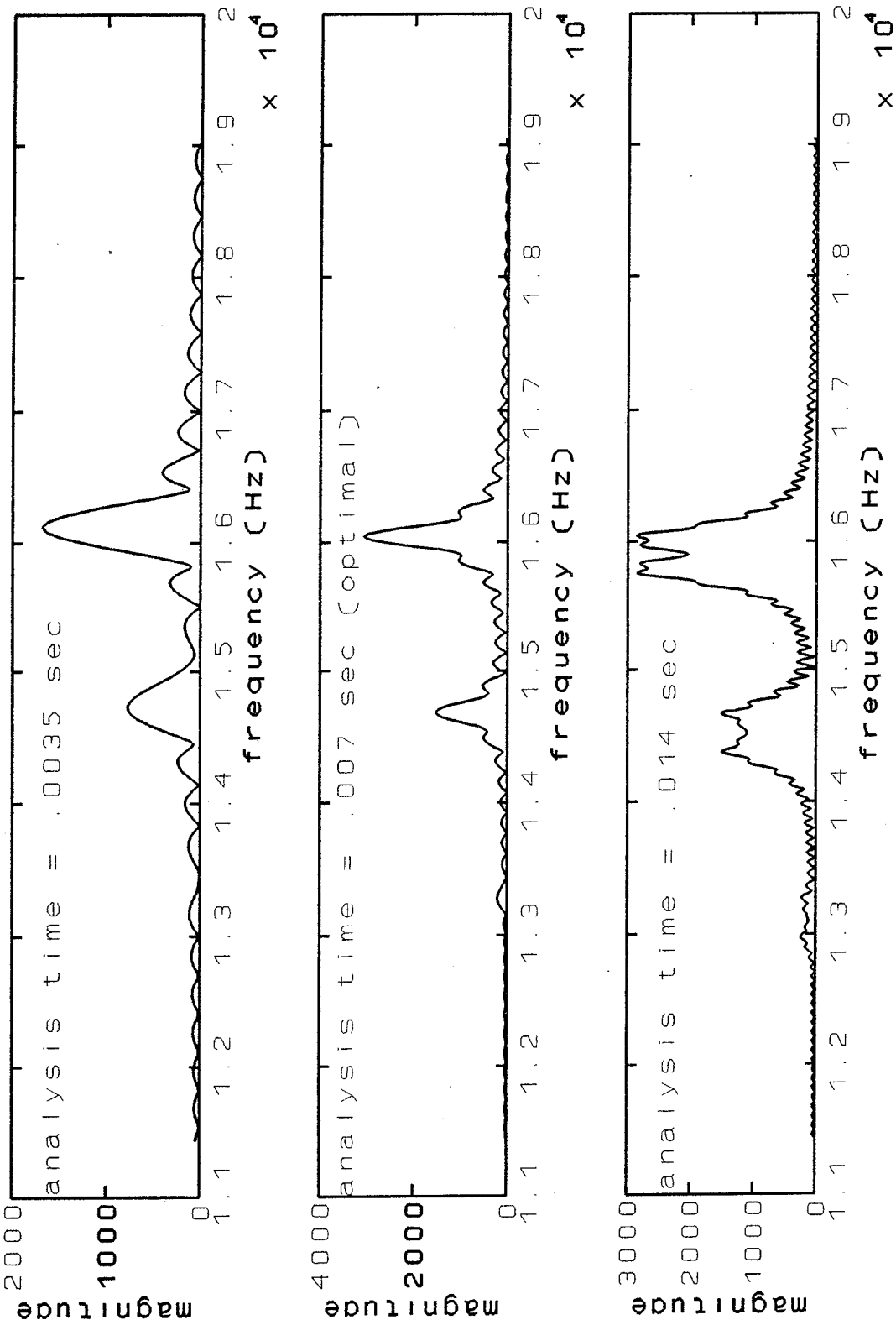Figure 5-8. Resolved Time-Frequency Display.

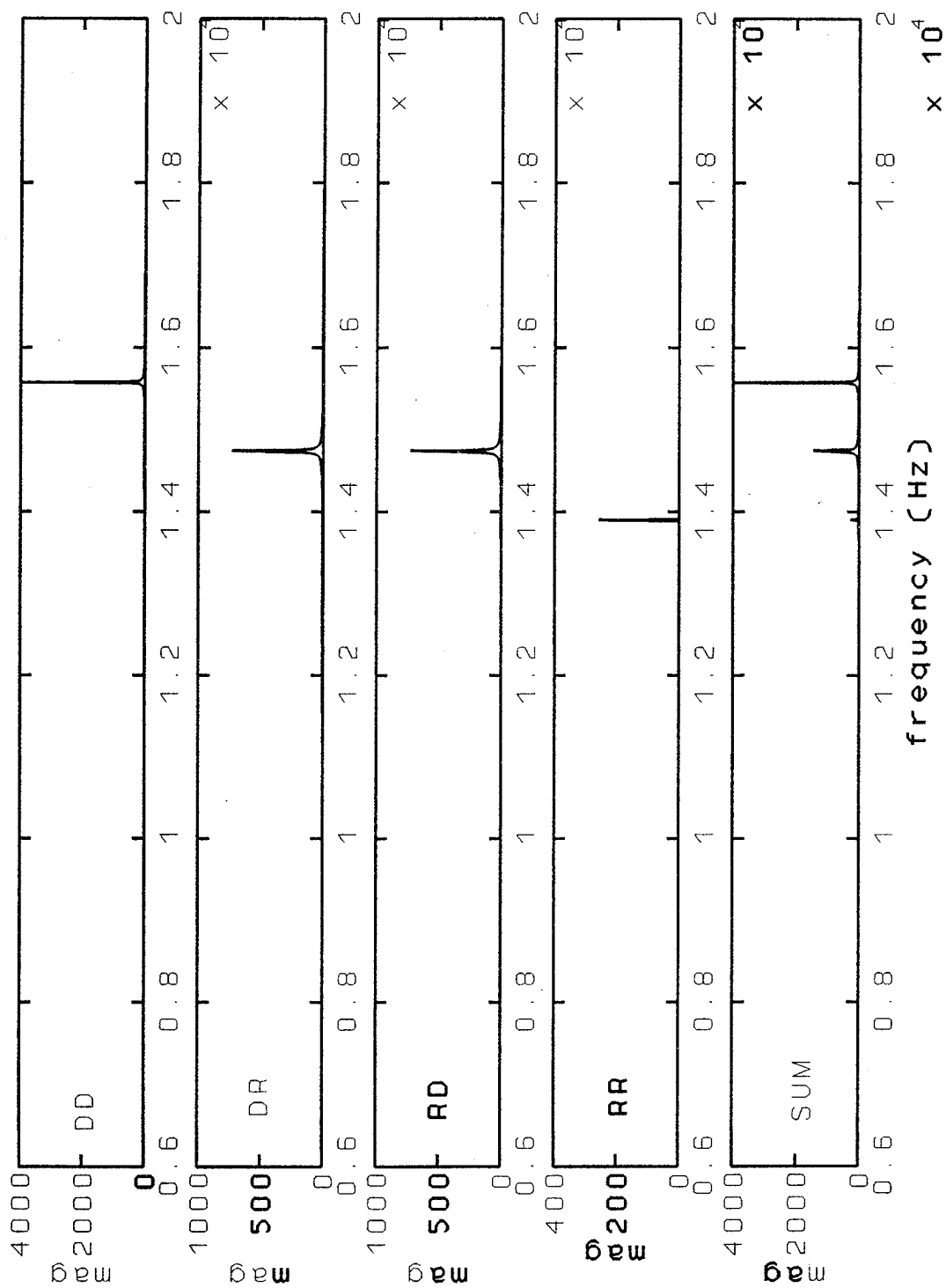Figure 5-9. Effect of Analysis Interval on Multipath Resolution

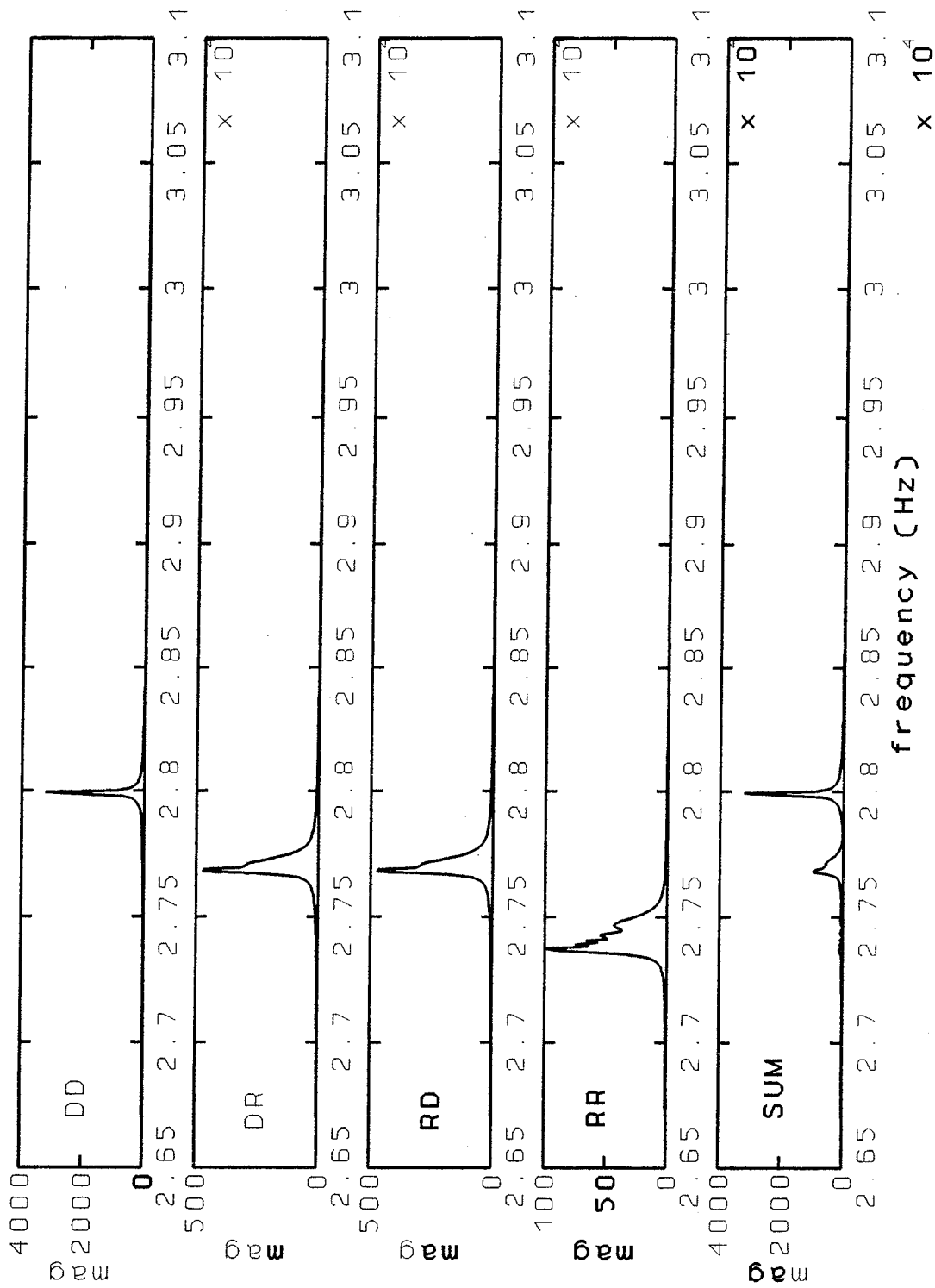Figure 5-10. Spectra of Constant-Range Target

Figure 5-11. Resolved Spectra of Spiraling Target and Image

CHAPTER 6

CONCLUSIONS AND RECOMMENDATIONS

Two methods were proposed for using W-band radar to get Doppler processing to enhance information on target motion. The first method involves detecting target maneuvers under a constant- speed assumption in conditions that are quite general. The second method involves determining target direction of motion relative to surfaces of constant PLD in some special circumstances. Several examples were presented to show under which conditions either method can be used advantageously. The simulations and analysis performed in this study indicate that the separate multipath lines are present in the spectrum, but that the signal processing methods based on the Discrete Fourier Transform will only rarely be able to resolve closely spaced multipath lines. However, the use of time- frequency signal processing techniques such as the Higher Order Ambiguity Function, the Cohen class transforms, and the Wavelet Transform[9] show some promise of being able to resolve the multipath lines.

When the special circumstances that allow the resolution of the multipath lines are present, a significant improvement in track determination is to be expected. The detection of the special circumstances using standard Fourier processing (*i.e.*, FFTs) has been reduced to the evaluation of a single parameter, P_{opt}, which can be estimated on line during the course of tracking. When this parameter is *comfortably* greater than unity, then the optimum analysis interval T_{opt} is computed. If T_{opt} is less than the dwell interval, then the multipath lines are resolvable with standard Fourier techniques and the corresponding computations are performed. Otherwise, P_2 is computed to see if the dwell interval is sufficiently long. If $P_2 > 1$, then the dwell interval is deemed long enough, and the computations are performed.

The capability to resolve the multipath lines may be enhanced by a technique of integrating several spectra over a short time interval. To accomplish this, it will be necessary to *align* the spectral peaks that are to be summed in magnitude. This will involve tracking of the frequency lines. Advanced frequency-line tracking techniques, such as a Hidden Markov Model-based algorithm (see Reference 10) may prove to be valuable for this application.

When the multipath lines are resolved, two techniques were discussed for enhancing the accuracy in the estimate of target state. First, the resolved skin line is essentially free of the effects of reflection at the sea surface. Thus, the monopulse ratio computed at the skin

Doppler frequency is relatively free of multipath effects. Secondly, the frequency separation of the resolved multipath lines provides an estimate of the path-length-difference rate. This information can serve as an additional measurement that can be incorporated into the measurement update process by means of the Extended Kalman Filter. Several subsequent studies are needed to translate the concepts of this report into practical methods. These can be enumerated as (1) pulse Doppler, (2) vibration, (3) noise, (4) time-frequency representation, and (5) implementation

The continuous-wave formulation used in this report does not provide an estimate of target range, which is of course essential to this and all other applications. *Pulse Doppler* provides range estimates, but introduces ambiguities in both range and frequency. The details of pulse Doppler and resolving the range and frequency ambiguities would need to be addressed.

An extended target has *vibrational modes*, which cause relative movement of the scattering points. The movement of the scattering points gives many different range rates, which vary with the phase of each mode. These effects may be comparable to or exceed the difference in range rates of the main target and its image. Quantitative studies are needed.

The simulations presented in this report have ignored the problem of noise. In an actual situation, diffuse sea-reflection noise, thermal noise in the electronic systems, and other noise sources would be present. To be useful in practice, the methods suggested in this report need to be shown practical in the presence of noise. Also, the amount of noise that can be tolerated without making these methods unworkable needs to be evaluated.

The *alignment* of spectral peaks discussed is in reality a way of making a time-frequency analysis. Other methods of time- frequency analysis, some of which have been mentioned, may provide better resolution of the multipath lines. The relative merits of these methods need to be studied in order to select one that is effective and computationally easy to apply.

After all the above issues have been considered, an algorithm for implementation of the multipath-line-splitting feature needs to be written and then tested by simulation and perhaps with real data.

CHAPTER 7

REFERENCES

1. Northam, D. Y., *A Stochastic Simulation of Low Grazing Angle, Forward Scatter, Over-Water Multipath Effects*, Naval Research Laboratory, Washington, DC, NRL Report 8568, 31 Dec 1981.

2. Gray, J. E., *A Note on the Doppler Effect for Non- Uniform Motion: A Canonical Representation of the Received Waveform*, (unpublished script, NSWCDD, 9 Aug 1994).

3. Durlach, N. I., *Influence of the earth's surface on radar*, Massachusetts Institute of Technology, Lincoln Laboratory, Technical Report No. 373, 18 Jan 1965.

4. Bar-Shalom, Y., Kumar, A., Blair, W. D., and Groves, G. W., "Tracking Low Elevation Targets in the Presence of Multipath Propagation," *IEEE Transactions on Aerospace and Electronic Systems*, Vol. 30, No. 3, Jul 1994, pp. 973-979.

5. Blair, W. D., Conte, J. E., and Rice, T. R., "Distortion Analysis of Signals Recovered Using Cepstral Processing," *Proc. of 1991 Conference on Information Sciences and Systems*, Mar 1991.

6. Gray, J. E., Rice, T. R., and Conte, J. E., "A Method for Determining the Non-Linear Time Dependence of Windowed Data Gathered from Scattered Signals," *Proc. IEEE-SP International Symposium on Time-Frequency and Time-Scale Analysis*, 4-6 Oct 1992, Victoria, B.C., Canada.

7. Atlas, L. E., and Marks, R. J., "Tutorial No. 1; Auditory Neural Systems and Time-Frequency Theory," *IEEE Conf. on Neural Networks for Ocean Engineering*, Washington, DC, 15-17 Aug 1991.

8. Pitton, J., Fox, W., Luby, J., and Loughlin, P., "Range- Doppler Processing with the Cone Kernel Time Frequency Representation," *Proc. IEEE Pac. Rim Conf. on Comm., Computers and Sig., Proc.*, Victoria, Canada, 9-10 May 1991, pp. 799-802.

9 Porat, B., "Digital Processing of Random Signals," *Prentice Hall Information and System Sciences Series*, Englewood Cliffs, NJ, 1994.

10. Xianga, Xie Evans, R. J., "Multiple Frequency Line Tracking Using Hidden Markov Models," *Proceedings of the 29th Conference on Decision and Control*, Honolulu, HI, Dec 1990.

DISTRIBUTION

COPIES

DOD ACTIVITIES (CONUS)

ATTN CODE 313 DR RABINDER MADAN OFFICE OF NAVAL RESEARCH 800 N QUINCY STREET ARLINGTON VA 22217	1
ATTN ONR 313 WILLIAM J. MICELI OFFICE OF NAVAL RESEARCH ARLINGTON VA 22003	1
ATTN E29L TECHNICAL LIBRARY COMMANDING OFFICER CSSDD NSWC 6703 W HWY 98 PANAMA CITY FL 32407-7001	1

NON-DOD ACTIVITIES

ATTN PROFESSOR YAAKOV BAR-SHALOM ESE DEPARTMENT U-157 260 GLENBROOK RD STORRS CT 06269-3157	1
ATTN PROFESSOR G. B. GIANNAKIS SCHOOL OF ENGINEERING AND APPLIED SCIENCE DEPARTMENT OF ELECTRICAL ENGINEERING UNIVERSITY OF VIRGINIA CHARLOTTESVILLE VA 22903-2442	1
ATTN DR RAMAN K MEHRA SCIENTIFIC SYSTEMS 500 W CUMMINGS PK SUITE 3950 WOBURN MA 01801	1
ATTN DR LEE SPENCE MASSACHUSETTS INSTITUTE OF TECHNOLOGY LINCOLN LABORATORY 244 WOOD STREET LEXINGTON MA 02173-9108	1

COPIES

THE CNA CORPORATION PO BOX 16268 ALEXANDRIA VA 22302-0268	1
DEFENSE TECHNICAL INFORMATION CENTER CAMERON STATION ALEXANDRIA VA 22304-6145	1
ATTN GIFT AND EXCHANGE DIVISION LIBRARY OF CONGRESS WASHINGTON DC 20540	4

INTERNAL DISTRIBUTION

B052	MOORE	1
B30	CAIN	1
B32	BLAIR	10
B32	GROVES	10
B32	CONTE	5
B32	RICE	1
B32	HELMICK	1
B32	GENTRY	1
B32	WATSON	1
B32	CHEN	1
E232		2
E282	GRAY	1
F	PENDERGRAFT	1
F406	HORMAN	1
F41	OSBORNE	1
F41	MARKER	1
F42	SOON	1
G73	MIMMS	1
N74	GIDEP	1

REPORT DOCUMENTATION PAGE

Public reporting burden for this collection of information is estimated to average 1 hour per response, including the time for reviewing instructions, search existing data sources, gathering and maintaining the data needed, and completing and reviewing the collection of information. Send comments regarding this burden or any other aspect of this collection of information, including suggestions for reducing this burden, to Washington Headquarters Services. Directorate for Information Operations and Reports, 1215 Jefferson Davis Highway, Suite 1204, Arlington, VA 22202-4302, and to the Office of Management and Budget, Paperwork Reduction Project (0704-0188), Washington, DC 20503.

1. AGENCY USE ONLY (*Leave blank*)	2. REPORT DATE October 1995	3. REPORT TYPE AND DATES COVERED

4. TITLE AND SUBTITLE

Preliminary Analysis of Vertical-Motion Detection for Low-Elevation Targets with Doppler Processing at W-Band

5. FUNDING NUMBERS

6. AUTHOR(s)

G. W. Groves   J. E. Conte   W. D. Blair

7. PERFORMING ORGANIZATION NAME(S) AND ADDRESS(ES)
Naval Surface Warfare Center
Dahlgren Division (Code B32)
17320 Dahlgren Rd.
Dahlgren, VA 22448-5100

8. PERFORMING ORGANIZATION REPORT NUMBER

NSWCDD/TR-94/351

9. SPONSORING/MONITORING AGENCY NAME(S) AND ADDRESS(ES)

10. SPONSORING/MONITORING AGENCY REPORT NUMBER

11. SUPPLEMENTARY NOTES

12a. DISTRIBUTION/AVAILABILITY STATEMENT

Approved for public release; distribution is unlimited.

12b. DISTRIBUTION CODE

13. ABSTRACT (*Maximum 200 words*)

The detection of vertical motion of a low-elevation target in multipath by frequency analysis using millimeter waves such as W-band radar is considered. Target vertical motion can be detected if the range rate of the image differs sufficiently from that of the target itself, so that their Doppler shifts allow resolution of the target return from its image. This observed difference in frequency provides additional information on target position and velocity. The favorable circumstances that create the possibility of using this effect to detect vertical target motion are discussed. An optimum interval in the time domain for analysis is developed for the case when the multipath-induced splitting of the Doppler-shifted frequencies is resolvable. A procedure is outlined for determining at each radar dwell (1) whether or not the multipath returns are resolvable, and (2) the appropriate analysis interval for achieving the resolution. A practical signal-processing technique is suggested for achieving the desired spectral resolution. Several examples of target trajectories are presented to illustrate cases where each method succeeds or fails. Conclusions and recommendations for further studies are given.

14. SUBJECT TERMS

W-Band Doppler   Kalman Process   Target Range   Path-Length Difference

15. NUMBER OF PAGES

42

16. PRICE CODE

17. SECURITY CLASSIFICATION OF REPORT	18. SECURITY CLASSIFICATION OF THIS PAGE	19. SECURITY CLASSIFICATION OF ABSTRACT	20. LIMITATION OF ABSTRACT
UNCLASSIFIED	UNCLASSIFIED	UNCLASSIFIED	SAR

NSN 7540-01-280-5500

Standard Form 298 (Rev 2-89)
Prescribed by ANSI std. Z39-18
298-102

GENERAL INSTRUCTIONS FOR COMPLETING SF 298

The Report Documentation Page (RDP) is used in announcing and cataloging reports. It is important that this information be consistent with the rest of the report, particularly the cover and its title page. Instructions for filling in each block of the form follow. It is important to *stay within the lines* to meet *optical scanning requirements*

Block 1. Agency Use Only (Leave blank).

Block 2. Report Date. Full publication date including day, month, and year, if available (e.g. 1 Jan 88). Must cite at least the year.

Block 3. Type of Report and Dates Covered. State whether report is interim, final, etc. *If applicable, enter inclusive report dates (e.g. 10 Jun 87 - 30 Jun 88).

Block 4. Title and Subtitle. A title is taken from the part of the report that provides the most meaningful and complete information. When a report is prepared in more than one volume, repeat the primary title, add volume number, and include subtitle for the specific volume. On classified documents enter the title classification in parentheses.

Block 5. Funding Numbers. To include contract and grant numbers; may include program element number(s), project number(s), task number(s), and work unit number(s). Use the following labels:

C	- Contract	PR	- Project
G	- Grant	TA	- Task
PE	- Program Element	WU	- Work Unit Accession No.

Block 6. Author(s). Name(s) of person(s) responsible for writing the report, performing the research, or credited with the content of the report. If editor or compiler, this should follow the name(s).

Block 7. Performing Organization Name(s) and address(es). Self-explanatory.

Block 8. Performing Organization Report Number. Enter the unique alphanumeric report number(s) assigned by the organization performing the report.

Block 9. Sponsoring/Monitoring Agency Name(s) and Address(es). Self-explanatory.

Block 10. Sponsoring/Monitoring Agency Report Number. *(If Known)*

Block 11. Supplementary Notes. Enter information not included elsewhere such as: Prepared in cooperation with...; Trans. of ,,,; To be published in... . When a report is revised, include a statement whether the new report supersedes or supplements the older report.

Block 12a. Distribution/Availability Statement. Denotes public availability or limitations. Cite any availability to the public. Enter additional limitations or special markings in all capitals (e.g. NOFORN, REL, ITAR).

DOD	-	See DoDD 5230.24, "Distribution Statements on Technical Documents"
DOE	-	See authorities.
NASA	-	See Handbook NHB 2200.2
NTIS	-	Leave blank

Block 12b. Distribution Code.

DOD	-	Leave blank.
DOE	-	Enter DOE distribution categories from the Standard Distribution for Unclassified Scientific and Technical Reports.
NASA	-	Leave blank.
NTIS	-	Leave blank.

Block 13. Abstract. Include a brief (*Maximum 200 words*) factual summary of the most significant information contained in the report.

Block 14. Subject Terms. Keywords or phrases identifying major subjects in the report.

Block 15. Number of Pages. Enter the total number of pages.

Block 16. Price Code. Enter appropriate price code (*NTIS only*).

Block 17-19. Security Classifications. Self-explanatory. Enter U.S. Security Classification in accordance with U.S. Security Regulations (i.e., UNCLASSIFIED). If form contains classified information, stamp classification on the top and bottom of this page.

Block 20. Limitation of Abstract. This block must be completed to assign a limitation to the abstract. Enter either UL (unlimited or SAR (same as report). An entry in this block is necessary if the abstract is to limited. If blank, the abstract is assumed to be unlimited.